



Review

Recent advances of graphene-based materials for high-performance and new-concept supercapacitors

Xiaoyu Shi^{a,b,c}, Shuanghao Zheng^{a,b,d}, Zhong-Shuai Wu^{a,*}, Xinhe Bao^{a,b}^a Dalian National Laboratory for Clean Energy, Dalian Institute of Chemical Physics, Chinese Academy of Sciences, 457 Zhongshan Road, Dalian 116023, Liaoning, China^b State Key Laboratory of Catalysis, Dalian Institute of Chemical Physics, Chinese Academy of Sciences, 457 Zhongshan Road, Dalian 116023, Liaoning, China^c Department of Chemical Physics, University of Science and Technology of China, 96 JinZhai Road, Hefei 230026, Anhui, China^d University of Chinese Academy of Sciences, 19 A Yuquan Road, Beijing 100049, China

ARTICLE INFO

Article history:

Received 20 September 2017

Revised 29 September 2017

Accepted 30 September 2017

Available online 10 October 2017

Keywords:

Graphene

Supercapacitors

Energy storage

High performance

New concept

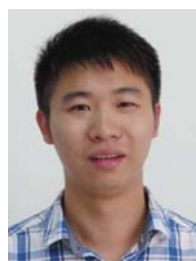
ABSTRACT

Supercapacitors, with ultrahigh power density, superior rate capability, long-term cyclability, and exceptional safety, are regarded as one highly competitive candidate of electrochemical energy storage devices, filling the gap between batteries and conventional capacitors. Despite of tremendous effort, elaborated screening of high-performance electrode materials, e.g., graphene, is still intensively required. In this review, we describe the most recent progress in the research and development of graphene-based materials for high-performance and new-concept supercapacitors for the targeted applications in next-generation and smart electronics. First, the design and fabrication of high-performance supercapacitors, including electrical double layer capacitors, pseudocapacitors and hybrid supercapacitors, were summarized in term of the charge storage mechanism. Second, new-concept supercapacitors with multiple functionalities of high-voltage, fiber-shape, microscale and shape-diversity in order to fulfill the requirements of future electronics are reviewed. Accordingly, special emphasis is given to the structure-dependent-performance effects of pores, hybridization, dimensionalities of graphene-based materials on performance of supercapacitors, and tremendous potential of graphene-based planar micro-supercapacitors for the direct seamlessly integration with versatile micro-electronics. Finally, perspectives and challenges of graphene-based supercapacitors are briefly discussed.

© 2017 Science Press and Dalian Institute of Chemical Physics, Chinese Academy of Sciences. Published by Elsevier B.V. and Science Press. All rights reserved.



Xiaoyu Shi received his B.S. degree from Nankai University in 2015. He is a Ph.D. candidate at University of Science and Technology of China, co-supervised by Prof. Xinhe Bao and Prof. Zhong-Shuai Wu. His current research focuses on 2D materials for flexible energy storage devices.



Shuanghao Zheng is now pursuing the Ph.D. degree from Dalian National Laboratory for Clean Energy, DICP, CAS, under the supervision of Prof. Xinhe Bao and Prof. Zhong-Shuai Wu. He obtained B.S. degree in Applied Chemistry from Changsha University of science & Technology in 2014. His research interests focus on graphene & 2D materials, supercapacitors and micro-supercapacitors.

* Corresponding author.

E-mail address: wuzs@dicp.ac.cn (Z.-S. Wu).



Zhong-Shuai Wu received his Ph.D. in materials science from Institute of Metal Research, CAS in 2011, and worked as a postdoctor at Max-Planck Institute for Polymer Research in 2011–2015. Then he joined DICP, CAS, and was appointed as full Professor, and group leader of 2D Materials & Energy Devices. He has published about 60 research articles in *Adv. Mater.*, *Nat. Commun.*, *J. Am. Chem. Soc.*, *ACS Nano* etc., with a total citation of more than 12,000 times. His research focuses on graphene and 2D materials for supercapacitors, micro-supercapacitors, batteries, flexible and microscale energy-storage devices. He is a recipient of Recruitment Program of Global Expert (1000 Talent Plan). He is guest editors of *Journal of Energy Chemistry*, *Energy Storage Materials*, and *Chinese Chemical Letters*, and corresponding expert of Engineering.

energy Chemistry, Energy Storage Materials, and Chinese Chemical Letters, and corresponding expert of Engineering.



Xinhe Bao received his Ph.D. in physical chemistry from Fudan University, China, in 1987. He moved to Germany in 1989 and worked as an Alexander von Humboldt Fellow at the Fritz-Haber Institute in Berlin. In 1995 he came back to China and joined the DICP as a full professor. He is a member of the Chinese Academy of Sciences, and a Fellow of the Royal Society of Chemistry. His research interest is nano and interfacial catalysis, and focus on the fundamental understanding of catalysis by nanotechnologies and in situ characterization techniques, and their applications to the development of new nanocatalysts and novel catalytic processes related to energy conversion and storage.

1. Introduction

With the rapid developments of portable electronics and hybrid electric vehicles, electrochemical energy storage devices (EESDs) have attracted more and more attentions to meet this ever-increasing demand. Lithium ion batteries, the most widely used EESDs, can not absolutely fulfill the diversified requirements in different practical situations taking into account of low power density (Fig. 1) [1]. On the other hand, electrolytic capacitors exhibit extremely high power density, but incapable of driving high-energy electronic devices.

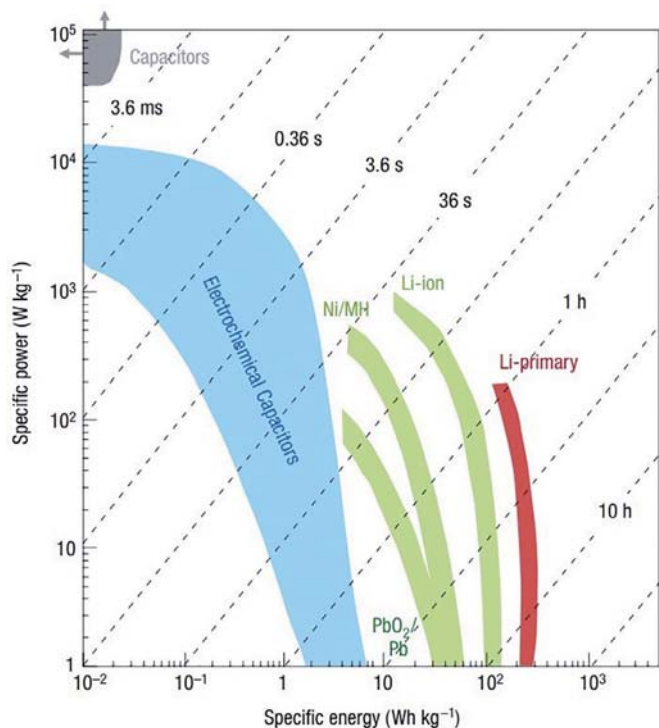


Fig. 1. Ragone plot of various electrical energy storage systems including electrolytic capacitors, supercapacitors and batteries. Reprinted from Ref. [1] with permission of Nature publishing group.

Supercapacitors (SCs), also called ultracapacitors or electrochemical capacitors, have drawn great attentions as promising next-generation power sources to fill the gap between electrolytic capacitors and batteries because SCs possess higher energy density than electrolytic capacitors, larger power density than batteries, superior cycle life ($> 10^5$ times), ultrafast charge and discharge processes (within several seconds or several minutes) [2–4]. According to charge storage mechanism, SCs are usually divided into electrical double layer capacitors (EDLCs), pseudocapacitors and hybrid SCs (HSCs, Fig. 2) [4,5]. EDLCs store energy through fast adsorption and desorption of electrolyte ions at the electrode surface, delivering high power density. Pseudocapacitors use fast and reversible surface and near surface redox reactions for charge storage, possessing high energy density. HSCs, consisting of an EDLC electrode and a pseudocapacitive electrode, can efficiently combine high power of EDLCs and high energy of pseudocapacitors. Besides the purpose of high energy density and power density, next-generation and new-concept SCs are becoming the main interesting direction to satisfy the needs of modern society and emerging flexible electronics, because such SCs possessing multi-functions of such as high voltage, shape diversity, miniaturization and fiber-shape can serve as efficient smart power sources that integrate seamlessly with these portable and wearable electronics [3,6–10]. Nevertheless, the key prerequisite to develop all these SCs lies in the designed fabrication of high-performance advanced electrode materials.

Graphene, a single-atom-thick, crystalline carbon film exhibiting various unprecedented properties [11], has attracted dramatic interest after the discovery by Novoselov et al. in 2004 [12]. Motivated by its outstanding electrical conductivity, high theoretical specific surface area (SSA) of $2620 \text{ m}^2/\text{g}$, excellent mechanical property and high theoretical capacitance of 550 F/g [13,14], considerable efforts are continuously devoted to developing graphene as novel electrode materials for high-performance and new-concept SCs [15–20].

Considering the explosive growth of research in this cutting-edge field, herein we summarize the most recent processes of graphene-based materials for high-performance SCs in details, emphasize the rational fabrication of graphene-based materials including graphene, porous graphene, graphene-polymer, graphene-metal oxide and hydroxide, graphene fibers and graphene films in different types of SCs (EDLCs, pseudocapacitors, and HSCs) and multifunctional smart SCs (high-voltage, fiber-shape, micro-scale, and arbitrary-shape), and describe the enormous potential of graphene-based SCs as advanced power sources integrated with multifarious portable, wearable and smart electronics and hybrid electric vehicles. Finally, perspectives and challenges of graphene-based SCs are also discussed how to design advanced graphene materials for next-generation high-performance SCs.

2. High-performance SCs

2.1. Graphene-based materials for EDLCs

Usually, EDLCs are composed of current collectors, two carbon electrodes, separator and electrolyte, as shown in Fig. 3(a) [21]. EDLCs store energy by reversible electrostatic adsorption and desorption of electrolyte ions at the surface of electrode materials and carbon materials are used as positive and negative electrodes. When a potential difference is applied between positive and negative electrodes, cations and anions in electrolyte will move towards different electrodes to keep charge balance, and inverse processes take place when SCs are discharged [4]. In general, the charge and discharge can be accomplished in an extremely short time and no chemical reaction is involved, thereby EDLCs present high power density and ultra-long cycle life.

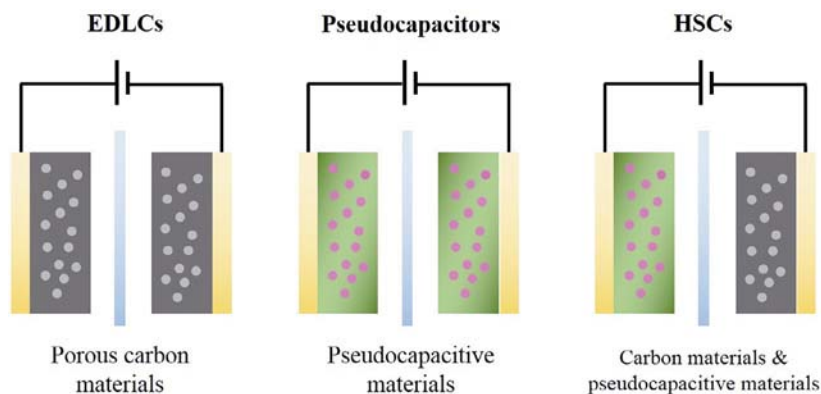


Fig. 2. Schematic of energy storage mechanism of EDLCs, pseudocapacitors and HSCs.

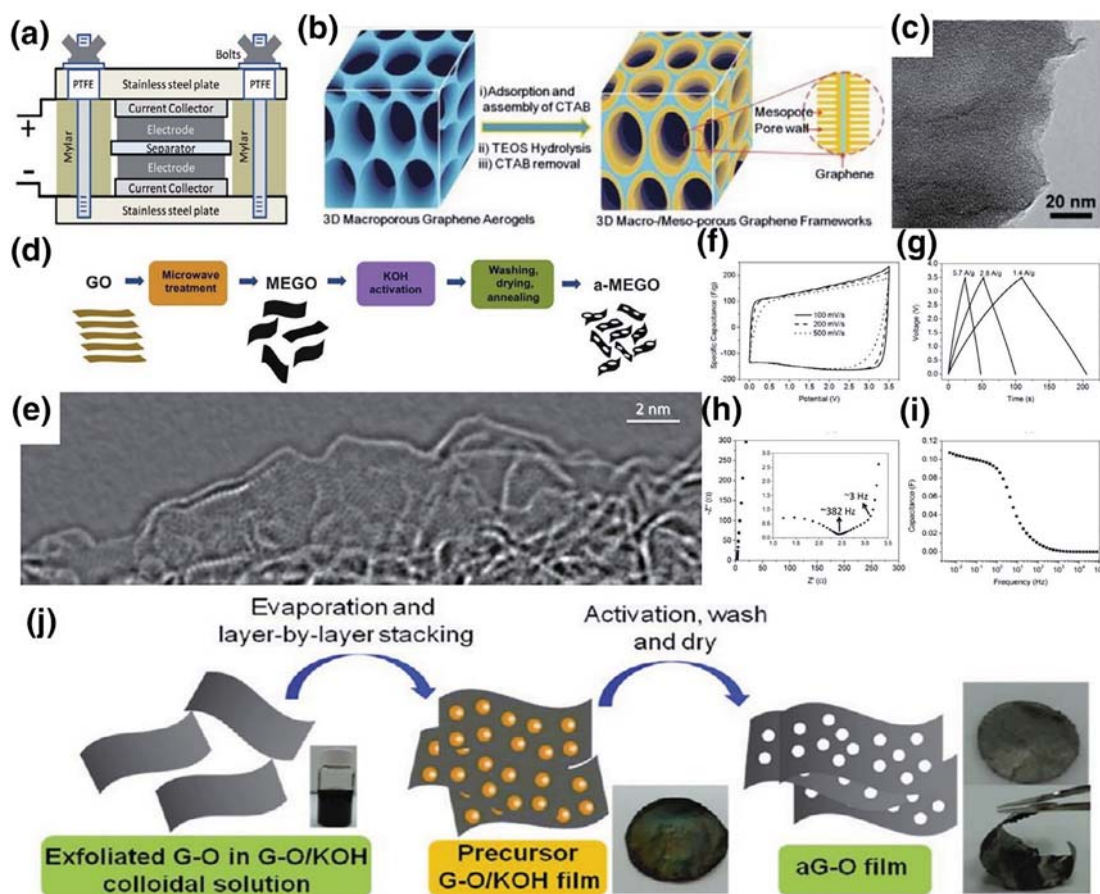


Fig. 3. (a) Schematic of test cell assembly of SCs. (b) Fabrication of hierarchical macro- and mesoporous GA-SiO₂ frameworks. (c) High resolution transmission electron microscopy (HRTEM) image of GA-MC. Reprinted from Refs. [21] and [22] with permission of American Chemical Society. (d) Fabrication schematic of MEGO and the following chemical activation of MEGO with KOH. (e) HRTEM image from the edge of a-MEGO. (f–i) Cyclic voltammetry (CV) curves, galvanostatic charge-discharge (GCD) profiles, Nyquist plot and frequency response of gravimetric capacitance of a-MEGO (SSA ~2400 m²/g) supercapacitor in EMIMBF₄/AN electrolyte. Reprinted from Ref. [15] with permission of AAAS. (j) Synthesis schematic of aG-O. Reprinted from Ref. [23] with permission of American Chemical Society.

2.1.1. High gravimetric capacitance porous graphene-based materials

High SSA of electrode materials plays a significant role in the enhancement of charge storage because electrostatic adsorption and desorption of electrolyte ions mainly take place on the surface of electrode. Graphene with high theoretical SSA is considered as ideal electrode materials for EDLCs. However, in practical situations the surface of graphene-based materials can not be utilized sufficiently due to serious stacking caused by strong Van der Waals' force between graphene sheets, resulting in relatively low specific gravimetric capacitance. To solve the problem, various

porous graphene materials with large SSA are fabricated to improve gravimetric capacitance of EDLCs [15,22–28]. For example, Wu et al. [22] used graphene aerogel (GA) as three-dimensional (3D) support and cetyltrimethylammonium bromide as soft template to fabricate 3D GA based mesoporous silica (GA-SiO₂) framework. Then, using SiO₂ in GA-SiO₂ as sacrificial template and sucrose as the carbon source, GA-mesoporous carbon (GA-MC) was successfully synthesized (Fig. 3b). The resulting 3D GA-MC frameworks exhibit narrow mesopore size distribution (2–3.5 nm) and high SSA (295 m²/g) (Fig. 3c). It was disclosed that interconnected

macropores are favorable to shorten the diffusion distances from electrolyte to surface of electrodes and mesopores in thin walls together with micropores derived from the stacked graphene sheets significantly enhance charge storage. Benefiting from the synergistic integration of meso- and macro-porous structures, GA-MC electrode for EDLCs manifested an outstanding specific capacitance of 226 F/g (at 1 mV/s), high rate capability, and excellent cycling stability without capacitance loss after 5000 cycles. Simultaneously, considering the prominent influence of doping to properties of graphene [29,30], Wu et al. [31] assembled SCs based on 3D nitrogen and boron co-doped GAs. The as-fabricated SCs possessed excellent electrochemical performance owing to porous 3D interconnected networks and enhancement of charge transport derived from heteroatom doping.

Another typical example of porous graphene applied in SCs with enhanced performance is porous graphene activated by KOH [15]. Ruoff's group developed a simple chemical activation of microwave exfoliated graphene oxide (a-MEGO) with KOH, and obtained activated graphene materials with ultrahigh SSA of 3100 m²/g that exceeds the theoretical SSA of graphene and most reported carbon materials activated by KOH [32,33], large pore volume up to 2.14 cm³/g, high electrical conductivity, low oxygen and hydrogen content. The chemical activation of MEGO presented a continuous 3D highly curved network, and the in-plane crystallinity was well preserved (Fig. 3e). In two-electrode systems with 1-ethyl-3-methylimidazolium tetrafluoroborate/acetonitrile (EMIMBF₄/AN) electrolyte, a-MEGO SCs displayed high specific capacitances of 165, 166, and 166 F/g at varying current densities of 1.4, 2.8, and 5.7 A/g and a superior energy density of ~70 Wh/kg. Following this work, Ruoff's group [23] further reported the fabrication of highly conductive and porous reduced GO (rGO) films through a simple solution evaporation, vacuum filtration and similar activation process (Fig. 3j). The as-synthesized activated reduced graphene oxide (aG-O) films had a highly porous and interconnected 3D microstructure, high SSA of 2400 m²/g, and remarkable electrical conductivity of 5880 S/m. The SCs using aG-O electrodes demonstrated excellent high-frequency response, and high-power delivery of ~500 kW/kg. Further, Chen's group [24] reported the simple and scalable synthesis of a new class of porous 3D graphene-based bulk materials, using hydrothermal polymerization and carbonization of the mixture of cheap biomass and GO, followed by chemical activation process. Benefiting from abundant mesopores, defected and wrinkled graphene sheets, ultrahigh SSA of 3523 m²/g, and high electrical conductivity of 303 S/m, the fabricated SCs displayed superior performance with high specific capacitance of 231 F/g and energy density of 98 Wh/kg in ionic liquid electrolyte.

It is noted that the design of novel porous graphene nanostructures in different dimensionalities is of great importance to increase the whole performance of SCs. For instance, Wei's group [34] developed the fabrication of 1D highly conductive graphene nanofibers (GNFs) by chemical vapor deposition (CVD) process involving the decomposition of MgCO₃·3H₂O template fibers to MgO fibers, deposition of carbon on the surface, and removal of MgO by acidic washing. The as-prepared GNFs exhibited high SSA of 1280 m²/g, good structural stability, and 3 times electrical conductivity of carbon nanotube (CNT) aggregates. The SCs using GNFs as electrodes and EMIMBF₄ as electrolyte operated at a wide voltage window of 0–4 V and exhibited high energy density in a wide range of power density.

2.1.2. High volumetric capacitance graphene-based materials

Compared to specific gravimetric capacitance, the volumetric capacitance is also a very important performance metrics to evaluate the practicability of SCs [35]. However, high SSA graphene materials are usually composed of shaggy sheets and have a low

packing density of less than 0.5 g/cm³, resulting in low volumetric capacitance and energy density. To overcome this issue, Yang et al. [16] fabricated the flexible liquid electrolyte-mediated chemically converted graphene (EM-CCG) films with high packing density of ~1.33 g/cm³, by compressing CCG hydrogel films at presence of nonvolatile electrolyte (Fig. 4a and 4b). The graphene sheets in the films were well stacked in a nearly face-to-face fashion, and the packing density could be readily tailored by modulating the ratio of volatile and nonvolatile liquids (Fig. 4c and 4d). More importantly, EM-CCG films created a continuous ion and electron transport network even at a high packing density. Hence, the SCs based on EM-CCG films obtained superior volumetric energy density of ~60 Wh/L, approaching the value of lead-acid batteries.

To solve the problem of porous graphene with a low packing density, Duan's group [36] developed a free-standing holey graphene framework (HGF) through one-step process with simultaneous low-temperature etching of nanopores in graphene by H₂O₂ and self-assembly of graphene into 3D network structure, and then compressed HGF to form a free-standing compact HGF film using a hydraulic press (Fig. 4e, 4f and 4h). The packing density of HGF films increased nearly 60-fold compared to HGF (from 1 cm thick HGF with a packing density of ~12 mg/cm³ to 140 μm thick flexible film with a packing density of ~0.71 g/cm³) (Fig. 4g). Because of abundant in-plane pores of a few nanometers, efficient electron and ion transport pathways, and high packing density, the HGF electrode delivered high volumetric capacitance of 212 F/cm³ in organic electrolyte, and the fully packaged device offered exceptional volumetric energy density of ~49 Wh/L. Similarly, Duan's group [38] also fabricated solution-processable holey GO (HGO). Compared to nanopore-free GO, HGO possessed abundant in-plane nanopores, which efficiently promoted ion diffusion and access to the graphene surface. Therefore, in 2 M EMIMBF₄ electrolyte, HGP-based SCs could deliver higher specific capacitance and better rate performance.

Notably, graphene and its analogue 2D nanosheets possess ultra-thin plane construction, providing the fast diffusion of electrolyte ions along the 2D planes in well-designed planar SCs, and consequently minimizing the resistance of ionic diffusion [39]. Inspired by this, Yoon et al. [37] developed a facile method to fabricate highly dense vertically aligned rGO (VARGO) through hand-rolling and cutting processes, as shown in Fig. 4(i). Benefiting from vertically aligned arrays, open-edge graphene structure, and high packing density of 1.33 g/cm³, the VARGO based SCs exhibited ideal capacitive behavior even at a high scan rate of 20 V/s, and delivered a high volumetric capacitance of 171 F/cm³, much higher than rGO powder and rGO film electrodes (Fig. 4l and 4m). Additionally, Ruoff's group [40] simply compressed a-MEGO based electrode material to achieve a volumetric capacitance of 110 F/cm³, using organic electrolyte in two-electrode systems. Yang's group [41] developed a facile evaporation-induced drying strategy to synthesize high density porous graphene macroform (HPGM) with a SSA of 370 m²/g, and high packing density of 1.58 g/cm³, significantly balancing two incompatible characteristics of both a porous microstructure and a high packing density. Therefore, the resulting SCs using HPGM electrodes endowed superior volumetric capacitance of 376 F/cm³ and energy density of 13.1 Wh/L in aqueous electrolyte.

2.2. Pseudocapacitors

Pseudocapacitors storage energy through rapid and reversible redox reactions at the surface and near-surface of electrodes [1]. Compared to EDLCs, pseudocapacitors can deliver higher specific capacitance and energy density. Pseudocapacitive materials include two categories of transition metal oxides/hydroxides (e.g. RuO₂, MnO₂, Co₃O₄, Ni(OH)₂) [22,42–47], and conducting poly-

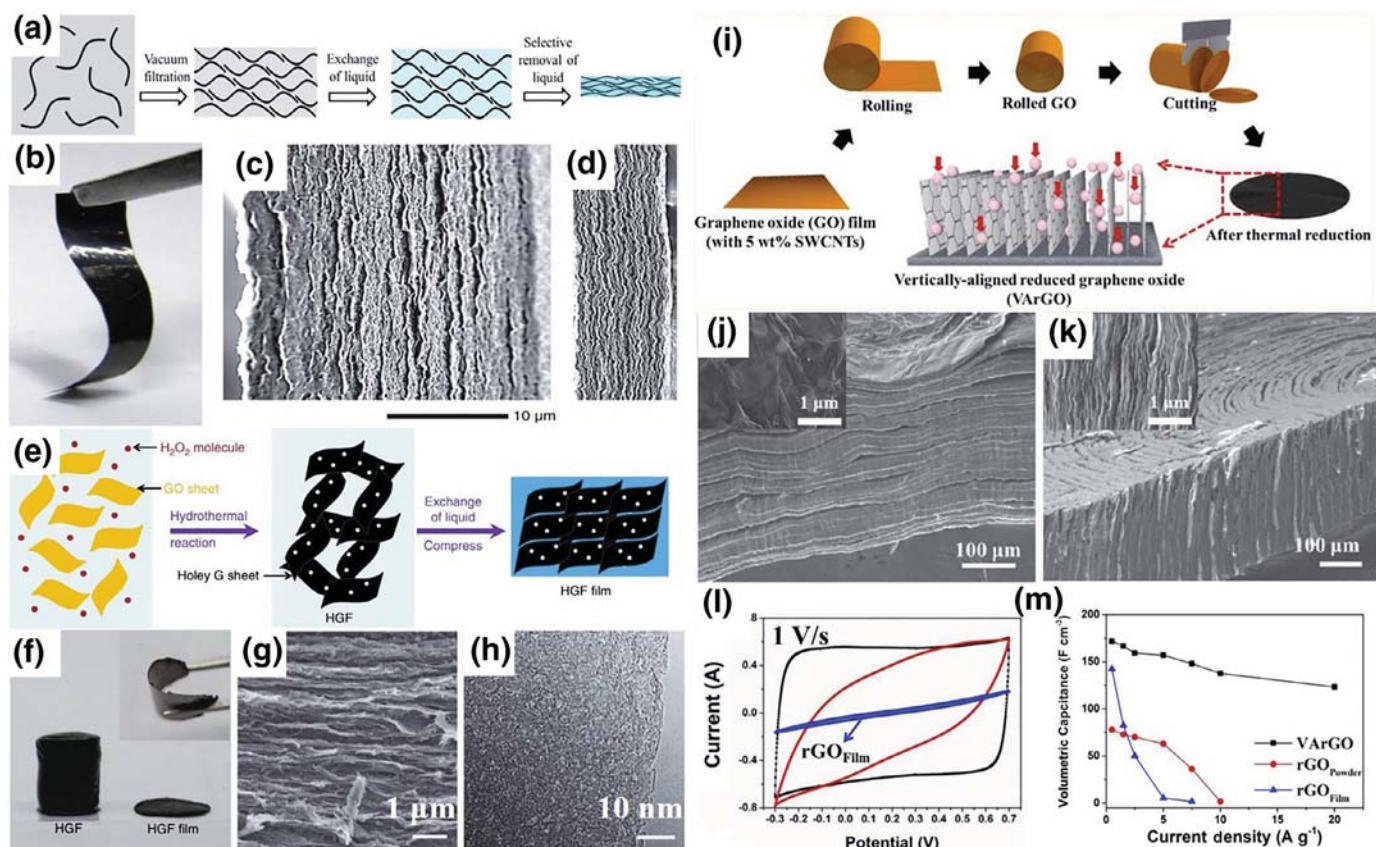


Fig. 4. (a) Schematic of fabrication of EM-CCG films from CCG dispersion. (b) Photograph showing the flexibility of the film. (c, d) Cross-section scanning electron microscopy (SEM) images of EM-CCG films containing 78.9% and 27.2% (vol%) of H_2SO_4 , respectively. Reprinted from Ref. [16] with permission of AAAS. (e) Schematic of the preparation process of HGF and HGF films. (f) A photograph of HGF before and after mechanical compression. (g) Cross-section SEM image of the HGF films. (h) TEM image of holey graphene sheets in HGF. Reprinted from Ref. [36] with permission of Nature publishing group. (i) Schematic of the fabrication of VArGO electrodes and electrolyte ions diffuse along the VArGO electrode sheets. (j, k) Cross-section SEM images of rGO film electrodes and VArGO electrodes. (l) CV curves of rGO powder, rGO film and VArGO electrodes at a scan rate of 1 V/s. (m) Volumetric capacitance as a function of current density of rGO powder, rGO film and VArGO electrodes. Reprinted from Ref. [37] with permission of American Chemical Society.

mers (e.g. polypyrrole (PPy), polythiophene and polyaniline (PANI), poly 3,4-ethylenedioxythiophene (PEDOT)) [48–53]. Unfortunately, poor electrical conductivity and incident volume change, resulting in low power density and short cycle life, limit their application as electrode materials for SCs. To address these issues, an efficient and general strategy is to construct their composite materials with graphene for the remarkable improvement of both rate performance and cyclability.

2.2.1. Graphene-conductive polymer hybrids

As a typical example, Wu et al. [49] developed a universal protocol for the construction of alternating stacked graphene-conductive polymer functionalized graphene hybrid films for high energy micro-supercapacitors (MSCs). Through an in-situ polymerization reaction, conductive polymer, e.g. PANI, PPy, was strongly anchored onto the surface of GO to form PANI-functionalized graphene (PANI-G) nanosheets and PPy-functionalized graphene (PPy-G) (Fig. 5b and 5c). Then, they fabricated alternating stacked graphene-PANI-G compact films through a layer by layer vacuum filtration of high-pseudocapacitive PANI-G (or PPy-G) nanosheets and high conducting electrochemically exfoliated graphene (EG) (Fig. 5d). The resulting hybrid films possessed high conductivity of 2120 S/m, large packing density of 1.67 g/cm^3 , and remarkable flexibility. Combining high capacitance of conductive polymer and outstanding electrical conductivity of EG nanosheets, the all-solid-state planar MSCs using the hybrid films as interdigital electrodes demonstrated landmark areal capacitance of 368 mF/cm^2 and vol-

umetric capacitance of 736 F/cm^3 (Fig. 5e and 5f). More importantly, the MSCs exhibited outstanding flexibility and performance stability, with slight capacitance loss after 1000 times under the bending operations (Fig. 5g and 5h). Subsequently, using the similar alternating stacking strategy, Wu et al. [50] fabricated stacked-layer heterostructure films of 2D thiophene nanosheets and EG nanosheets for high-rate and flexible all-solid-state MSCs, which exhibited a pronounced pseudocapacitive behavior with strong redox peaks, and high volumetric capacitance of 375 F/cm^3 . More importantly, these MSCs could be operated at high rate of up to 1000 V/s, and delivered stable performance under different bending states.

To construct the structurally-defined mesoporous polymer-graphene nanosheets, Liu et al. [48] developed a versatile route to synthesize GO-based mesoporous conductive polymers (mPPy@GO or mPANI@GO) nanosheets by using block copolymer polystyrene-*b*-poly(ethylene oxide) (PS-*b*-PEO) as the soft template (Fig. 5i). The strategy allows for bottom-up patterning of PPy and PANI with adjustable mesopores on diverse 2D materials including GO, molybdenum sulfide and titania nanosheets. As a typical example, the resulting mPPy@GO with adjustable pore sizes (Fig. 5j–m) and thickness exhibited remarkable specific capacitance of 383 F/g as electrodes for SCs.

2.2.2. Graphene-metal oxide and hydroxide hybrids

Due to the high specific capacitance, metal oxide and hydroxide have attracted more and more attentions as pseudocapacitive

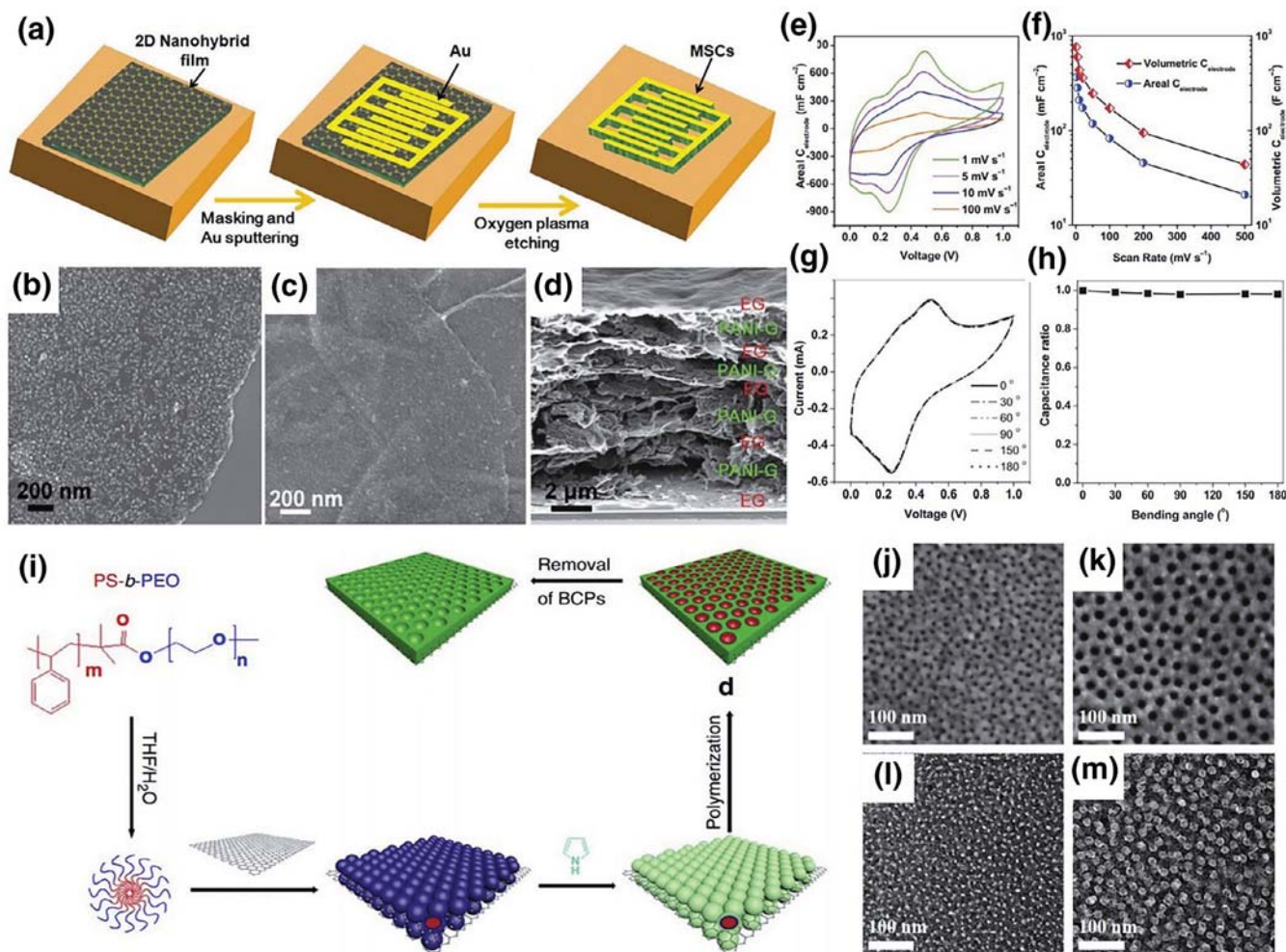


Fig. 5. (a) Illustration of the fabrication procedure for planar MSCs with interdigital fingers. (b, c) SEM images of PANI-G nanosheets and PPy-G nanosheets. (d) Cross-section SEM image of 2D hybrid films based on PANI-G and EG nanosheets. (e, f) CV curves, areal and volumetric capacitance of 2D hybrid film for MSCs. (g) CV curves of 2D hybrid films for MSCs bended with different angles at 10 mV/s. (h) Evolution of the capacitance ratio as a function of bending angle. Reprinted from Ref. [49] with permission of Wiley & Sons, Inc. (i) Schematic of patterning of 2D surfaces with mesoporous conductive polymer. (j, k) SEM images of mesoporous PPy@GO (mPPy@GO) with different PS block units of 38 and 102. (l, m) TEM images of mPPy@GO with different PS block units of 38 and 102. Reprinted from Ref. [48] with permission of Nature publishing group.

materials. For instance, Wu et al. [22] fabricated 3D graphene-metal oxide composite including GA-Co₃O₄ and GA-RuO₂ by infiltration of GA-SiO₂ in 2-isopropanol solution containing cobalt or ruthenium acetylacetonate, followed by heating and NaOH etching. The resulting GA-RuO₂ showed high specific capacitance of 560 F/g in three-electrode systems. Qin et al. [45] used a universal mask-assisted vacuum filtration to fabricate all-solid-state MSCs with MnO₂ nanosheets as pseudocapacitive materials, EG as current collectors and LiCl/polyvinyl alcohol (LiCl/PVA) as gel electrolyte. The resulting MSCs exhibited remarkable areal capacitance of ~355 mF/cm². It is worth noting that, in most cases, graphene-metal oxide and hydroxide materials are widely used for asymmetric SCs to enhance the output of voltage and energy density.

2.3. Hybrid supercapacitors

Although plentiful efforts have been devoted to increasing the performance of EESDs, the energy density of SCs and power density of batteries are still very limited, both of which hardly satisfy the urgent requirements of large-scale energy applications such as electric vehicles. HSCs, consisting of hybrid electrodes or asymmetric electrodes, have been acknowledged as promising candidates to bridge the gap between SCs and batteries. Such HSCs generally

combine high power density and long cycle life of SCs and high energy density of batteries [1,4]. So far, the most widely studied HSCs are aqueous electrolyte-based asymmetric SCs (ASCs), Li ion HSCs (Li-HSCs), and Na ion HSCs (Na-HSCs).

2.3.1. Graphene-based materials for aqueous ASCs

Considering the facts that energy density of SCs is proportional to the square of output voltage [54], and some electrical components such as diodes can not work when the voltage is lower than a critical value, therefore, increasing the voltage of SCs is highly required to improve the availability and practicability of SCs. Though the theoretical value of water electrolysis is 1.23 V in aqueous electrolytes [55], the voltage windows of ASCs could be widened to 1.4–2.4 V with the help of high oxygen evolution overpotential and low hydrogen evolution overpotential [42–44,55–60]. As mentioned above, in most cases metal oxide and hydroxide are used as electrodes for ASCs due to their high pseudocapacitance and wide voltage window. However, originating from their limited conductivity and stability, metal oxides and hydroxides can not be used directly as electrodes generally. As a result, synthesizing graphene-metal oxide and hydroxide hybrid as electrodes is considered as a good choice to assemble high-performance ASCs.

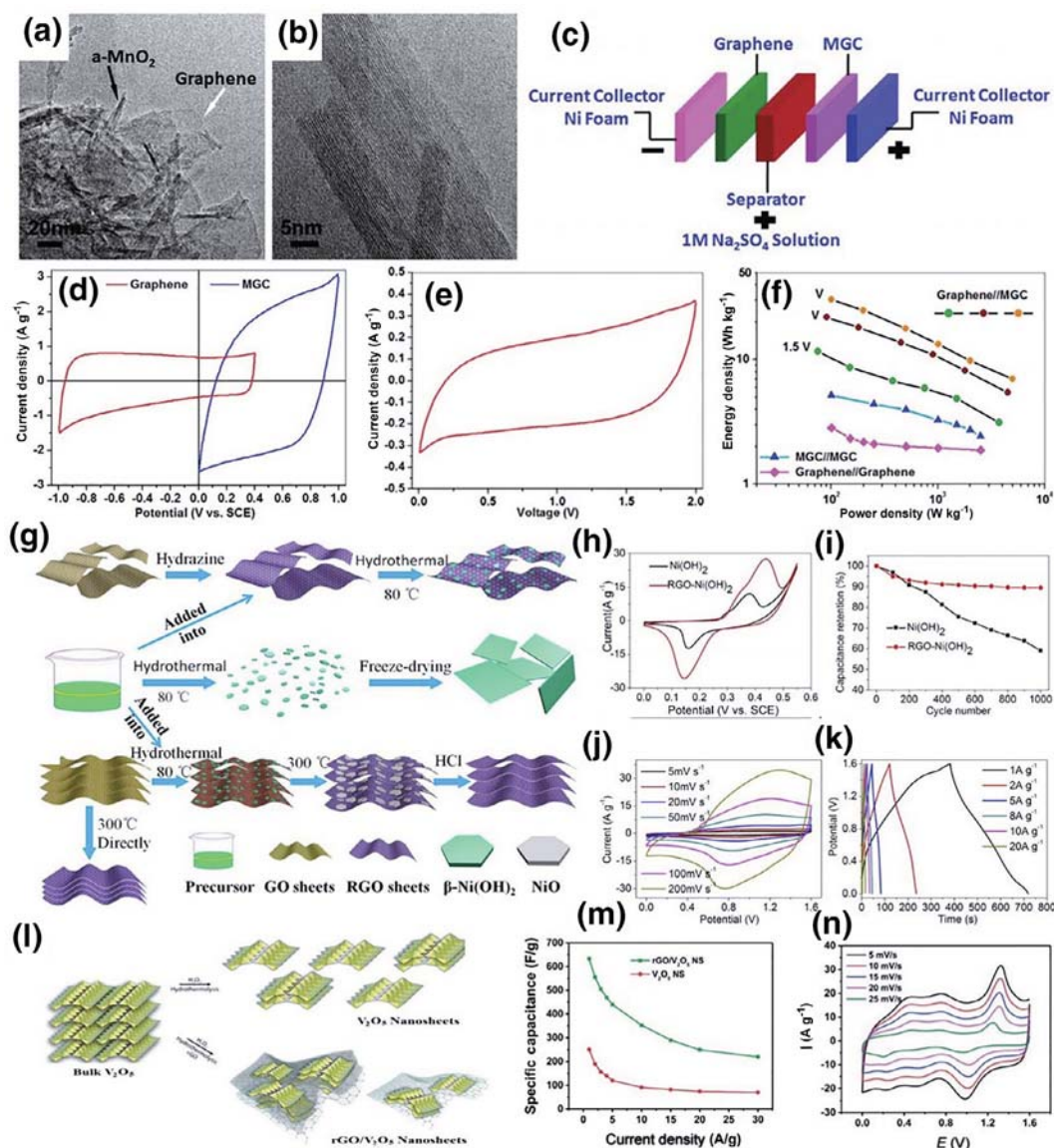


Fig. 6. (a) TEM image of MGC. (b) HRTEM image of the α -MnO₂ nanowires in MGC. (c) Schematic of the assembled structure of ASCs based on MGC as positive electrode and graphene as negative electrode. (d) CV curves of graphene and MGC electrodes performed in three-electrode systems with 1 M Na₂SO₄ aqueous solution at a scan rate of 10 mV/s. (e) CV curves of graphene//MGC ASCs with a voltage of 2 V at a scan rate of 10 mV/s. (f) Ragone plot of graphene//MGC ASCs with various voltage, graphene//graphene and MGC//MGC symmetric SCs. Reprinted from Ref. [42] with permission of American Chemical Society. (g) Schematic of the synthesis process of rGO-Ni(OH)₂ composite, pure Ni(OH)₂ and enhanced rGO sheets with Ni(OH)₂ particles as spacers. (h) CV curves at a scan rate of 5 mV/s and (i) specific capacitance as a function of current density of pure Ni(OH)₂ and rGO-Ni(OH)₂ composite. (j, k) CV curves and GCD profiles of rGO-Ni(OH)₂//rGO ASCs. (l) Schematic of hydrothermal synthesis of V₂O₅ and rGO/V₂O₅ nanosheets. (m) Specific capacitance as a function of current density of V₂O₅ and rGO/V₂O₅. (n) CV curves of activated rGO//rGO/V₂O₅ ASCs in aqueous 1 M KCl solution. Reprinted from Ref. [44] with permission of Royal Society of Chemistry.

Due to low-cost, abundant and environmentally friendly advantages, manganese oxides have been considered as one of the most promising positive electrode materials for ASCs [55,58,61,62]. As a pioneering work, Wu et al. [42] prepared MnO₂ nanowires/graphene composite (MGC) through solution-phase assembly of graphene and α -MnO₂ nanowires and further developed ASCs using MGC as positive electrode and graphene as negative electrode (Fig. 6a–6c). They firstly evaluated electrochemical properties of graphene and MGC respectively in three-electrode systems, tested in 1 M Na₂SO₄ (Fig. 6d). As shown in three-electrode systems, graphene and MGC could exhibit stable performances at potential windows of -1.0 – 0.4 V (vs. SCE) and 0 – 1.0 V (vs. SCE), respectively. Hence, the constructed ASCs with MGC as positive electrode and graphene as negative electrode exhibited stable performance at a wide voltage window of 0 – 2.0 V (Fig. 6e), and high

energy density of 30.4 Wh/kg, much higher than those of symmetric graphene//graphene SCs (2.8 Wh/kg) and MGC//MGC SCs (5.2 Wh/kg). It should be highlighted that this work paved a route to use graphene-metal oxide composites as electrode materials for applications in safe aqueous electrolyte-based high-voltage ASCs with high energy and power densities.

Ni(OH)₂ is another kind of electrode materials studied widely due to its high theoretical capacitance and low-cost [63–65]. Through a simple hydrothermal process Liu et al. [43] developed rGO-Ni(OH)₂ composite and enhanced rGO followed by annealing and HCl etching (Fig. 6g). In this case, rGO sheets were employed as suitable substrates to anchor Ni(OH)₂ nanoparticles against agglomeration and Ni(OH)₂ nanoparticles act as sacrificial spacers within rGO sheets to effectively reduce the irreversible restacking of rGO. Consequently, the resulting rGO-Ni(OH)₂ composite

exhibited superior specific capacitance of 1717 F/g, much higher than pure Ni(OH)₂ (Fig. 6h and 6i). Meanwhile, the enhanced rGO delivered high specific capacitance of 182 F/g at an ultrahigh current density of 100 A/g. The ASCs using rGO–Ni(OH)₂ and enhanced rGO as positive and negative electrodes respectively possessed a wide voltage window of 0–1.6 V, and delivered ultrahigh energy density of 75 Wh/kg and power density of 40,000 W/kg (Fig. 6j and 6k).

Besides, V₂O₅ is also widely used as a promising pseudocapacitive material due to natural abundance, low cost and multivalence states [66,67]. For instance, Nanaraju et al. [44] fabricated the rGO/V₂O₅ nanosheets (rGO/V₂O₅) through a universal hydrothermal reaction of mixture of bulk V₂O₅ solution and GO (Fig. 6l). Benefiting from the synergistic effect of graphene and V₂O₅ nanosheets, the rGO/V₂O₅ electrode showed high specific capacitance of 635 F/g at a current density of 1 A/g, much higher than 2D V₂O₅ nanosheets (253 F/g) (Fig. 6m). Further, the ASCs with activated rGO and rGO/V₂O₅ as negative and positive electrodes respectively output a voltage of 1.6 V and high energy density of 79.5 Wh/kg (Fig. 6n).

2.3.2. Graphene-based materials for Li-HSCs

Due to outstanding intrinsic properties of high SSA, high conductivity and abundant pore-structures for electron and ion transport, graphene materials could be directly used as electrodes for Li-HSCs. Typically, Yang's group [68] fabricated Li-HSCs using Li₄Ti₅O₁₂/carbon (LTO/C) and porous graphene macroform (PGM) as negative and positive electrodes, respectively (Fig. 7a–7c). The resulting Li-HSCs delivered a superior energy density of 72 Wh/kg, much higher than the values of PGM/PGM SCs and LTO//commercial activated carbon Li-HSCs (LTO//YP-17D) (Fig. 7d and 7e). Moreover, the LTO/C//PGM Li-HSCs exhibited good stability with 65% retention after 1000 cycles. Due to prominent difference among carbon-based materials, two kinds of different carbon materials could be used to assemble Li-HSCs sometimes. Kang's group [69] fabricated all-graphene Li-HSCs using functionalized graphene as positive electrode and rGO as negative electrode without requirement of lithium metals (Fig. 7f). Benefiting from fast surface reactions in both electrodes, the all-graphene Li-HSCs could output a high voltage of 4.5 V, and deliver a remarkably high power density 6450 W/kg while maintaining a high energy density of 225 Wh/kg, which was well comparable to conventional Li ion batteries (Fig. 7g and 7h).

Fabricating graphene-based hybrid electrode materials with boosted electrical conductivity is another efficient strategy to improve performance of SCs [71]. For example, Chen's group [72] developed a graphene-inserted LTO composite (G-LTO) anode through a simple solvothermal reaction, followed by annealing treatment. The as-prepared G-LTO delivered superior excellent reversible capacitance of 207, 190 and 176 mAh/g at rates of 0.3, 0.5 and 1 C respectively, higher than the theoretical value of 175 mAh/g for pure LTO. Furthermore, Li-HSCs consisting of G-LTO anode and 3D porous graphene-sucrose cathode delivered an ultrahigh energy density of 95 Wh/kg at a rate of 0.4 C. More importantly, it could still retain an energy density of 32 Wh/kg at a high rate of 100 C, indicating the effect of graphene to improve rate capacitance of electrode materials for Li-HSCs. Similarly, Cui's group [73] demonstrated graphene decorated with molybdenum dioxide nanoparticles (G-MoO₂) exhibited better performance than pure MoO₂ particles. The specific capacitance of the G-MoO₂ containing 10% graphene could reach 624.0 F/g, much higher than 269.2 F/g for the MoO₂ particles alone.

2.3.3. Graphene-based materials for Na-HSCs

Due to natural abundance, low cost and high theoretical capacitance, sodium has been extensively explored as a potential al-

ternative of lithium for HSCs. Currently, great efforts have been devoted to developing advanced electrode materials for Na-HSCs [74–76]. Similar to Li-HSCs, one common method to improve Na-HSCs is to accelerate the kinetics of battery-type electrodes in charge-discharge processes through developing graphene-based hybrid materials. As an important example, Lee's group [70] developed a facile synthesis of Nb₂O₅@C/rGO composites. Benefiting from the introduction of rGO, the aggregation of Nb₂O₅@C nanoparticles dispersed on the rGO surface could be significantly restrained during the insertion/extraction of Na ions. Therefore, the Nb₂O₅@C/rGO delivered a high specific capacity of ~285 mAh/g at 0.025 A/g, much higher than Nb₂O₅@C and commercially available Nb₂O₅ (com-Nb₂O₅). Further, Na-HSCs based on Nb₂O₅@C/rGO anode and MSP-20 cathode exhibited a remarkable energy density of ~76 Wh/kg and a power density of ~20,800 W/kg (Fig. 7i–7k). To address the leakage issue of liquid electrolyte, Wang et al. [77] demonstrated quasi-solid-state Na-HSCs, using a sodium ion conducting gel polymer electrolyte, based on nanoporous carbon nanoparticles and macroporous graphene as the negative and positive electrodes, respectively. The resulting Na-HSCs could operate at a voltage as high as 4.2 V, and possess ultrahigh energy density of 168 Wh/kg. More importantly, the safety and application have been improved significantly by using gel electrolyte in place of liquid electrolyte.

3. New-concept supercapacitors with diverse functions

As the rapid developments of new-generation portable, wearable, woven and smart electronics including smart watches, electric skins, micro-robots, sensors and so on [78–82], SCs are urgently required to possess extra functions for seamless integration with advanced electronics, the most important part for which is to develop new-type electrode materials. In this section, we will summarize graphene-based materials for new-concept smart SCs with diverse functions of such as high voltage, fiber shape, micro-scale and arbitrary shape, from material designs to device configurations.

3.1. Graphene-based materials for tandem high-voltage SCs

From the perspective of device design, connecting multiple SC devices in series is one efficient method to boost the output voltage [83,84]. As a typical example, Chen's group [85] designed and fabricated an internal tandem supercapacitor (ITSC) based on graphene-based porous carbon hybrid material as electrodes, EMIMBF₄ or 1 M tetraethylammonium tetrafluoroborate (TEABF₄) as electrolyte (Fig. 8a). Benefiting from increased weight proportion of the electrode materials in the whole device and wide voltage window of EMIMBF₄, the ITSC successfully output a high voltage of 7 V, and delivered a significantly improved energy density of 36.3 Wh/kg, increased by 33% compared to single cell supercapacitor (SCSC) (Fig. 8b–8e). More importantly, the ITSC also exhibited remarkable flexibility, cycle stability and rate performance. Similarly, Chen et al. [86] fabricated graphene- and graphene/PANI-based SCs through electrode deposition onto the both sides of a commercial separator, and then connected multi-devices in series to make tandem SCs (Fig. 8f and 8g). The as-prepared tandem SCs demonstrated ideal tandem behaviors and triple output voltage of single device.

Besides sandwich-like tandem SCs, in-plane tandem SCs has been also developed tremendously. Recently, our group [87] fabricated interdigital MSCs with graphene and phosphorene as electrodes through one-step vacuum filtration strategy with assistance of an interdigital patterned mask (Fig. 8j and 8k). Using 1-butyl-3-methylimidazolium hexafluorophosphate (BMIMPF₆) as electrolyte, the single cell operated a high voltage of 3 V, and impressively, the

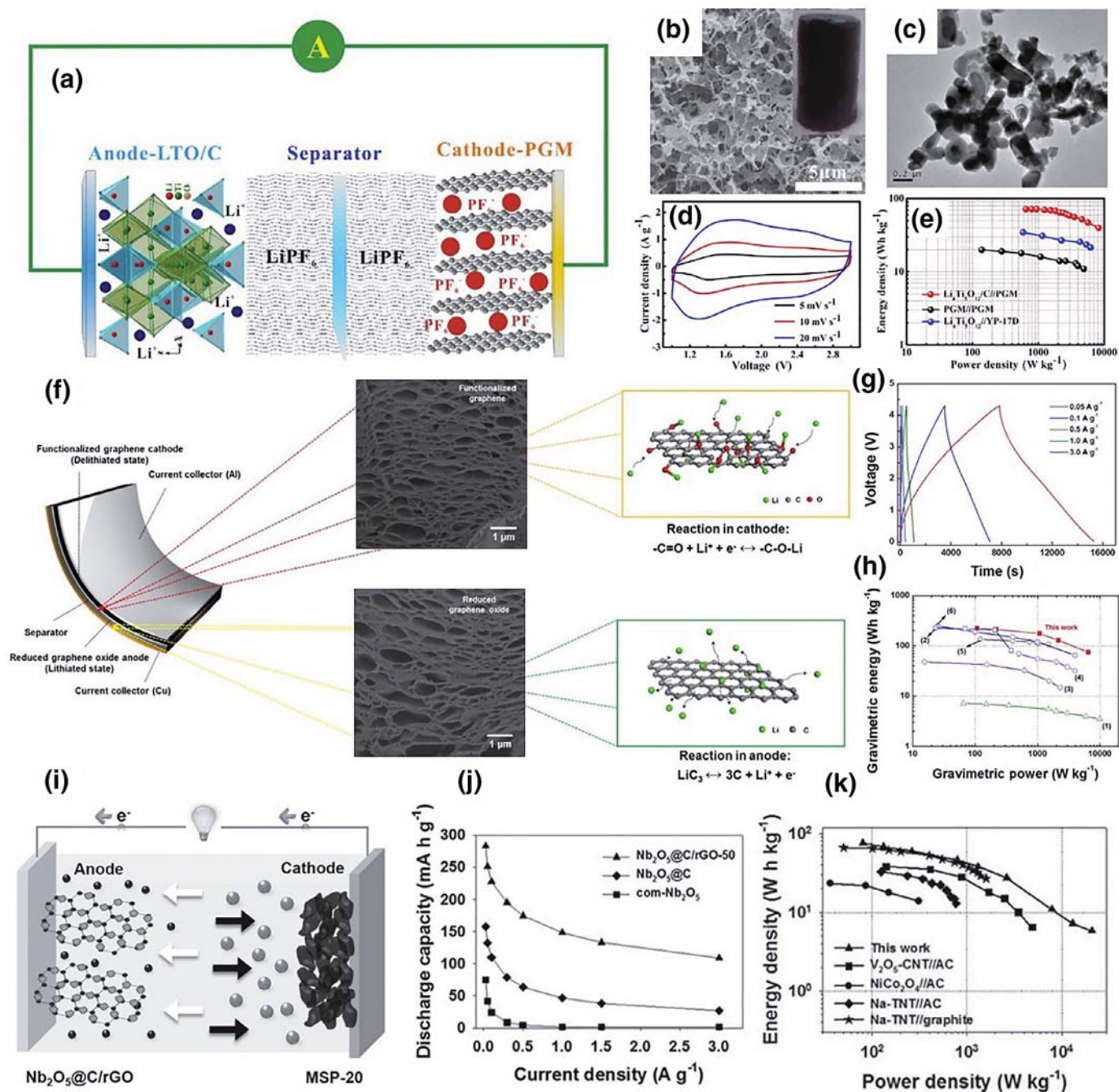


Fig. 7. (a) Schematic of Li-HSCs using PGM as positive electrode and LTO/C hybrid as negative electrode. (b) SEM image of the PGM and the inset is a photograph of PGM. (c) TEM image of the as-prepared LTO/C hybrid. (d) CV curves of LTO/C//PGM Li-HSCs performed at different scan rates. (e) Ragone plot of LTO/C//PGM Li-HSCs, PGM//PGM SCs and LTO//YP-17D Li-HSCs. Reprinted from Ref. [68] with permission of Elsevier. (f) Schematic of all-graphene Li-HSCs and its electrochemical reaction. (g) GCD profiles of all-graphene Li-HSCs at different current densities. (h) Ragone plot of all-graphene Li-HSCs and other EESDs. (i) Schematic of Na-HSCs systems composed of Nb₂O₅@carbon nanoparticles and rGO (Nb₂O₅@C)/rGO anode and activated carbon (MSP-20) cathode. (j) Discharge capacity of Nb₂O₅@C/rGO-50, Nb₂O₅@C and com-Nb₂O₅ at various current densities. (k) Ragone plot of the as-prepared Na-HSCs and other EESDs. Reprinted from Ref. [70] with permission of Wiley & Sons, Inc.

tandem device pack interconnected 3 MSCs in series output a high voltage of 9V, without additional metal-based interconnects and contacts (Fig. 8I and 8m).

3.2. Graphene-based fibers for supercapacitors

Fiber-based SCs (FSCs), as a new type of SCs, possess huge advantages of power and energy densities, flexibility, stretchability, wearability and fatigue resistance, which have been considered as one of the most promising candidates for the extensive application

of flexible and wearable electronic devices [88–90]. Moreover, the unique one-dimensional structure and strongly mechanical flexible characteristic of FSCs enable them to be easily weaved to yarns and fabrics with tailored size and shapes, which can be compatibly integrated with the flexible and wearable devices. Among various carbon fibers, graphene-based fibers (GFs) have demonstrated significant advantages over conventional carbon fibers and CNT fibers in the aspect of high strength, electrical and thermal conductivities and cost effective process due to the outstanding intrinsic chemical and physical features of graphene [91–95], such as excellent flex-

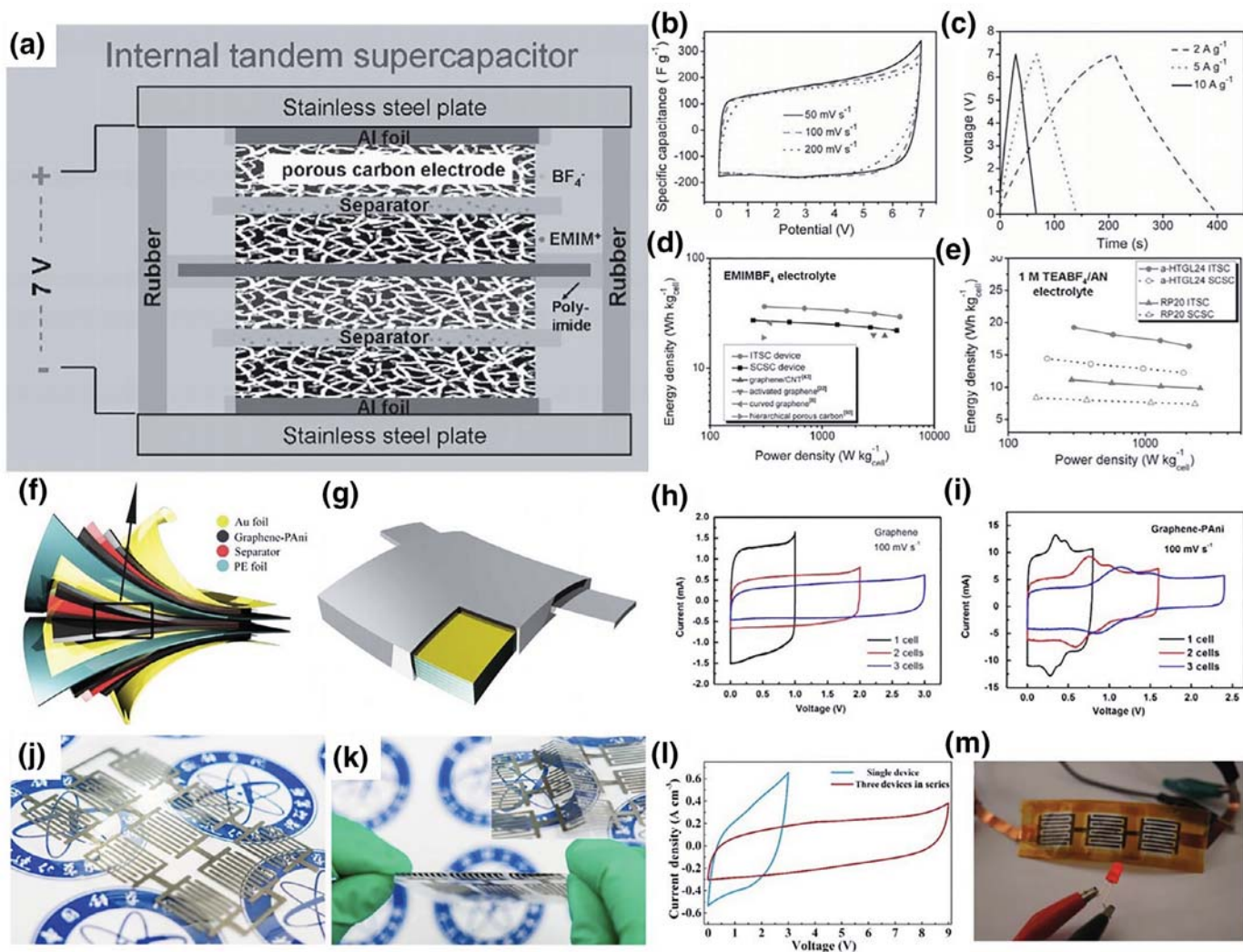


Fig. 8. (a) Schematic diagram of ITSC assembly design based on graphene-based porous materials. (b, c) CV curves and GCD profiles of ITSC at a voltage window of 0–7 V in EMIMBF₄ electrolyte. (d, e) Ragone plot of ITSC and SCSC in EMIMBF₄ and 1 M TEABF₄/AN based on different electrode materials. Reprinted from Ref. [85] with permission of Wiley & Sons, Inc. (f, g) The interior and exterior structures of the integrated tandem SCs. (h, i) CV curves of graphene- and graphene/PANI-based tandem SCs at a scan rate of 100 mV s⁻¹. Reprinted from Ref. [86] with permission of Elsevier. (j, k) Photographs of 9 serially interconnected phosphorene nanosheets and EG based-MSCs (PG-MSCs). (l) CV curves of single and three serial PG-MSCs tested at a scan rate of 100 mV s⁻¹. (m) Photograph of three serial PG-MSCs powering a light-emitting diode (LED). Reprinted from Ref. [87] with permission of American Chemical Society.

ibility and extraordinary stability. To date, great efforts have been devoted to maximizing their comprehensive performance of FSCs. By virtue of the unique architecture, excellent conductivity, favorable mechanical flexibility and outstanding electrochemical properties, GFs have been demonstrated to be a novel type of flexible fiber electrode materials for assembling high-performance FSCs.

3.2.1. Preparation of graphene fibers

Recently, various approaches have been creatively exploited for the fabrication of one-dimensional GFs, such as wet-spinning [92], hydrothermal treatment [96,97], electrophoretic assembly [98], film conversion [99], and substrate-assisted reduction and assembly (Fig. 9a–9c) [100]. Among them, the wet-spinning strategy can usually produce the massive and continuous GO fibers from liquid crystalline GO dispersions. As shown in Fig. 9(d), the wet-spinning technology is usually involved into three different stages, including flowing GO dope, self-standing GO gel and dried GO fiber [101]. In the stage I, liquid crystalline GO dopes flowed through spinning pipes under the extrusion forces, resulting in changing GO liquid crystalline from the random orientation to the induced uniform alignment. This oriented alignment is attributed to ki-

netic resistance of GO liquid crystalline along the flow direction. In the stage II, solvent exchange has occurred between GO liquid crystalline from spinning pipes and coagulator at the coagulation baths. After that, GO liquid crystalline gel fibers are achieved with the structural integrity remained thanks to strong Van der Waals' force between GO nanosheets or ion crosslinking interaction. In the stage III, GO gel fibers shrink and the diameter becomes smaller due to the evaporation of water between GO nanosheets. Finally, to convert GO fibers to GFs, reduction strategies in chemistry or physics are further required, then GFs with extraordinary mechanical strength, high electric and thermal conductivities are obtained [91,102]. Notably, the concentration of GO solution, size of GO nanosheets and spinning pipes, ingredient of coagulation bath, as well as the techniques of spinning play key roles in the fabrication and properties of GFs. In addition, GO liquid-crystalline solution can act as an effective host for various additive species, such as CNTs, metal nanowires (Cu nanowire and Ag nanowire), and conducting polymers (PANI and PPy). Therefore, tremendous graphene-based composite fibers with multifunctional properties have been fabricated. It should be mentioned that GFs with distinct architecture can be prepared via modifying the structure of the

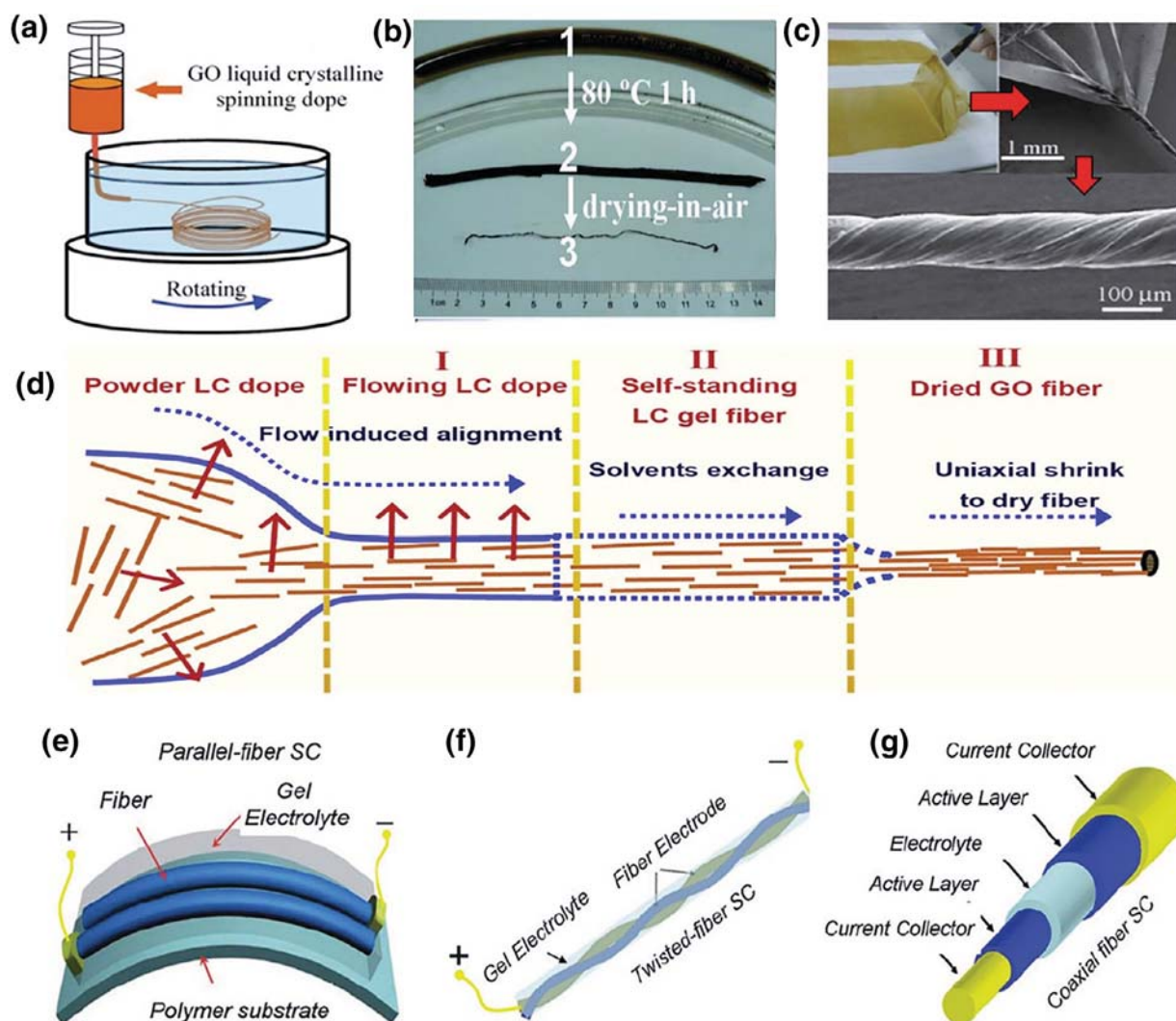


Fig. 9. (a) Wet-spinning approach to fabricate GO fibers in a rotating coagulation bath. Reprinted from Ref. [92] with permission of Wiley & Sons, Inc. (b) An optical image exhibiting the formation of GFs through hydrothermal treatment. Reprinted from Ref. [97] with permission of Royal Society of Chemistry. (c) The fabrication of GO fibers from twisting a long-strip GO film, which was cut from a GO film after evaporating the solvent from GO solution. Reprinted from Ref. [99] with permission of American Chemical Society. (d) Schematic of the wet-spinning process of the fabricated GO fibers, showing the clear assembled process of GO fibers from powder GO dope with random orientation to the self-standing gel fiber in a coagulation bath under the help of the induced alignment of uniaxial flow during the spinning. Reprinted from Ref. [101] with permission of Elsevier. (e–f) Three typical device configurations of FSCs: (e) two parallel fibers on the same substrate, (f) two twisted fibers, and (g) single coaxial fiber. Reprinted from Ref. [88] with permission of Royal Society of Chemistry.

spinneret and altering the composition of coagulant, such as hollow, porous, core-shell, various cross-section (triangle, Y-shaped, trefoil, four leaf, pentagon) shaped GFs [101,103,104]. Meanwhile, this wet-spinning technology also has some shortcomings, such as extra post processing for transforming GO fibers into GFs, and the difficulty of completely removing residues of inorganic or organic ions from surfaces of graphene nanosheets. Compared to the wet-spinning method, the dimensionally confined hydrothermal strategy can directly fabricate GFs with only one step and intrinsically defeat these disadvantages mentioned above. The resulting fibers usually have relatively high electrical conductivity and robust mechanical strength without further chemical or physical reduction treatment. Note that the foreign fillers can also be introduced into the GO solution to form the precursor for the fabrication of hybrid GFs. However, due to the strong dependency on the pre-designed pipeline, this method suffers from the size and length of the fabricated GFs, which is not suitable for practical application. Moreover, the process including sealing tube terminals and heating at high temperature for hours, makes it inappropriate for continuous

fabrication of GFs. Other methods, electrophoretic assembly, film conversion and substrate-assisted reduction and assembly, are also alternative approaches for the formation of high-performance GFs.

The excellent flexibility, high electronic conductivity and tractable properties of GFs endow them to be intensively employed as promising electrode materials of FSCs. The SC configuration based on GFs can be classified into three types of parallel, twisted and coaxial designs (Fig. 9e–9g) [88]. Among them, the parallel FSCs (Fig. 9e) are constructed with two parallel fibers on the same planar substrate using empty interspace between two fibers as separator. Such FSCs can be readily scaled up by integrating the fiber electrodes in series or parallel on the planar substrate to modulate the output power and energy, as a result, to meet the requirement of microscale electronics. However, the application of the planar substrate may restrict their wearable applications of FSCs. Inversely, both twisted and coaxial fibers with one-dimensional configuration don't require a planar substrate. The twisted FSCs (Fig. 9f) are assembled by twisting two fibers into the double helix structure with a separator or solid state

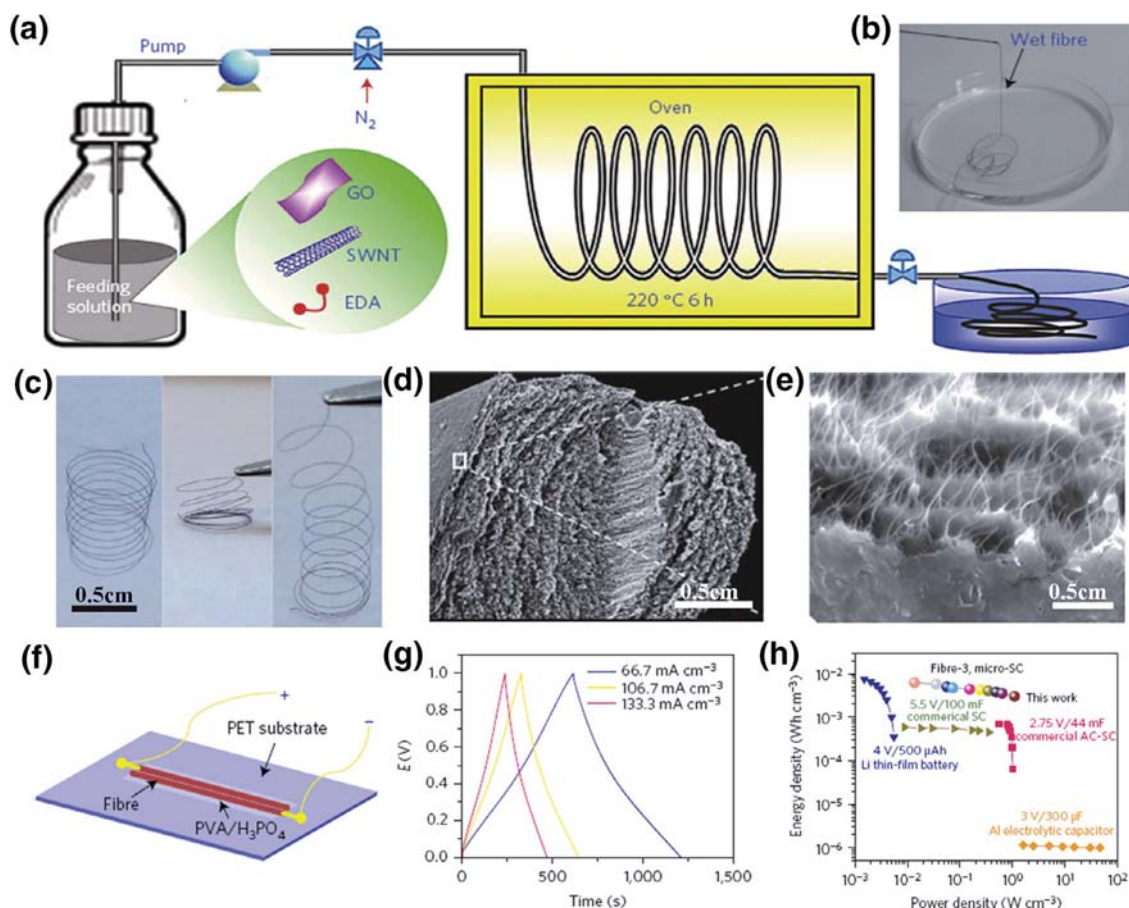


Fig. 10. (a) Schematic of the integrative fabrication of graphene and CNT hybrid microfibers through in situ thermal treatment. (b) Photograph of the as-fabricated fiber collected at water. (c) Photograph of the compressed and stretched fiber. (d) Cross-section SEM image of the as-prepared fiber. (e) SEM image with high magnification showing the square area in (d). (f) Schematic diagram of FSCs assembled with two fibers at the same flexible substrate. (g) GCD profiles at different current densities. (h) Ragone plot of the assembled FSCs in comparison with some commercial devices. Reprinted from Ref. [96] with permission of Nature publishing group.

electrolyte between them. On the other hand, the coaxial FSCs (Fig. 9g) are fabricated through layer-by-layer assembling from a core fiber to a separator and then an outer fiber. So far, various GF electrodes with multifunctional properties for FSCs have been explored, including pure GFs [105], graphene-CNT fibers [96,106,107], graphene-conducting polymer hybrid fibers [108], graphene-carbon fibers [109], and graphene-metal oxide fibers [110] as described below.

3.2.2. Graphene-based fiber supercapacitors

Recently, Chen's group and Dai's group [96] developed a linear hydrothermal micro-reactor to fabricate a hierarchically structured carbon microfiber composing of aligned single-walled CNT and nitrogen-doped rGO (Fig. 10). The homogeneous precursor solution of GO, CNT and ethylene diamine as a nitrogen dopant was injected by a pump into a flexible silica capillary with in situ hydrothermal treatment, and then N-doped graphene-CNT hybrid fibers were achieved (Fig. 10a and 10b). The resultant fibers presented robust flexibility (Fig. 10c), mesoporous structure with high SSA of 396 m²/g, and electrical conductivity of 102 S/cm (Fig. 10d and 10e). The assembled MSCs, based on these two parallel fibers on one planar substrate, showed high specific volumetric capacitance of 300 F/cm³ in PVA/H₃PO₄ and outstanding volumetric energy density of 6.3 mWh/cm³, which can be compared to that of thin film lithium batteries (Fig. 10f–10h). These excellent results are ascribed to the hierarchically structured N-doped graphene-CNT fibers. Meng et al. [10] designed twisted FSCs through intertwining 3D porous network-like graphene-based fibers. The fabri-

cated FSCs exhibited highly flexible, compressible and stretchable properties, and could be readily woven into a fabric for flexible or wearable electronics. In addition, Kou et al. [105] exploited a coaxial wet-spinning assembling strategy to fabricate polyelectrolyte-wrapped GFs using a double-inlet spinneret, in which GO was the inner spinning dope and sodium carboxymethyl cellulose as polyelectrolyte was fed to the sheath. The existence of polyelectrolyte sheath on the surface of GFs prevented the SCs from the electrolyte leakage when the devices were seriously deformed. Thereby, the core-sheath FSCs were flexible, wearable and robust enough to maintain the long-term and repeated deformation without degradation of the capacitance after 1000 cycles.

Conducting polymers, such as PANI, PPy, and PEDOT, are widely applied for fabricating graphene hybrid fibers for FSCs, accompanied with enhanced the mechanical strength, flexibility and capacitance performance. For instance, Wang et al. [111] prepared high-performance fiber-shaped SCs by doping PANI fibers with GO sheets. The assembled FSCs fabricated by intertwining two composite fibers delivered a high specific capacitance of 531 F/g, which was ascribed to the synergetic effect of the PANI and GO. Additionally, transition metal oxides, such as MnO₂, RuO₂ and Co₃O₄, have been intensively used as flexible electrode materials for FSCs. For example, Li et al. [110] fabricated the all-solid-state FSCs with two GFs modified by MnO₂ nanoparticles, exhibiting high areal capacitance of 42.0 mF/cm² at 10 mV/s, which was much higher than that of pure GFs (1.4 mF/cm²).

Graphene-based FSCs with their unique advantages of the superior flexibility and wearability have attracted widespread at-

tention, and have made much progress. However, the application of these graphene FSCs still faces several huge challenges. First, graphene FSCs just have high performance in small-scale measurement. Regarding their practical applications in an industrial level, it will take tremendous efforts to achieve high-performance, chemical and electronic stable devices. Second, besides the flexibility and capacitance, the stretchability of GFs is also the crucial factor for manufacturing flexible and wearable SCs. Third, at present, most graphene-based FSCs with limited voltage window in symmetric type cannot meet the demand of high voltage and high energy density. Therefore, the exploitation of asymmetric graphene-based FSCs in both aqueous and organic electrolyte is one of the key ways to improve electrochemical performance. Fourth, in wearable applications, safety is the greatest concern for users because of the corrosive electrolyte in use. To consider the future development of device, developing green nontoxic electrolyte for the safety of the FSCs will be one of the most significant directions. Last but not the least, large scale production of FSCs, including high conductivity and quality of GFs, is one of the biggest challenges in the future development of electronics.

3.3. Graphene films for micro-supercapacitors

3.3.1. Graphene-based MSCs

The current trend of miniaturized portable electronic equipment, microrobots, micro-electromechanical system and implantable medical devices, with multifunctional, flexible and highly integrated properties intensively leads to the ever-increasing demands for the efficient, microscale and compact on-chip energy storage systems [4,112–114]. However, the conventional energy storage systems, for example, SCs and lithium ion batteries, are difficult to meet multifunctional requirements and miniaturize in size and shape [49,115]. Moreover, micro-batteries suffer from short lifetime and low power density, which limit their widely practical application on fast charge-discharge process, even though they can provide high energy density [14,50,116]. Conversely, the emergence of new-typed on-chip MSCs which are composed of two electrodes, current collector, separator and electrolyte on a planar substrate, are well compatible with microscale integrated circuits to satisfy the requirements of the power source of micro-electronics [18,113,117]. Furthermore, the planar MSCs show tremendous desirable properties, e.g., ultrafast charge-discharge process, high power density, exceptional rate capability, outstanding frequency response, and ultra-long cycling stability. These superb characteristics, key for future application of miniaturized electronics, are attributed to the high-speed accessibility of the electrolyte to electrodes in planar structure and low ion transport resistance due to the lacking separator and short interspace between positive and negative electrodes [118]. Recently, graphene is demonstrated to be of great significance for MSCs owing to the brilliant match between the planar configuration of graphene and in-plane geometry of MSCs for maximizing the electrochemical capacitive behaviors, in which electrolyte ions can transfer along the planar structure of graphene [119–122]. In particular, the channels in porous graphene, including micro-, meso-, and macro-porous structure in either graphene planes or between graphene sheets, can extraordinarily enhance the available surface area of electrodes, decrease ion transfer resistance [15,22], and eventually enlarge the electrochemical performance of MSCs. Despite numerous progresses on MSCs, further improving their electrochemical performance is still urgent to realize their practical applications.

3.3.2. Graphene films for MSCs

Graphene is a promising and attractive electrode material for SCs, but the overall electrochemical performance of graphene-based SCs, especially the output power density, has not been fully

developed. In this regard, Müllen's group [17] exploited a new class of graphene-based planar interdigital MSCs on both rigid and flexible substrates using the CH_4 plasma to reduce GO, followed by oxygen plasma etching to fabricate finger patterns (Fig. 11a and 11b). The rGO film showed superior electrical conductivity of 345 S/cm and high C/O ratio of 9.2, since CH_4 plasma can provide additional carbon source to repair the defect of GO. As a result, the fabricated all-solid-state MSCs using the reduced graphene exhibited an ultrahigh scan rate up to 1000 V/s, which is at least three orders of magnitude higher than that of conventional SCs (Fig. 11c). This remarkable result indicated that this device can complete charge-discharge process in several milliseconds. Furthermore, the as-fabricated MSCs delivered high volumetric power density of 495 W/cm³, and excellent cycling stability. These outstanding outcomes are ascribed to the high electrical conductivity of graphene film and in-plane interdigital electrodes in the micro-devices, allowing for ultrafast adsorption-desorption of electrolyte ions from the graphene layers in a short diffusion pathway (Fig. 11d). To realize scalable fabrication and enhance the rate capabilities of graphene-based MSCs, a rational way is to facilitate the electrolyte accessibility of the active electrodes and avoid the restacking of graphene sheets. Typically, Kaner's group [123,124] reported the fabrication of porous graphene films with robust mechanical strength and large SSA of 1520 m²/g, which were achieved by the direct reduction of the tight restacked GO films using a standard Light Scribe DVD optical drive. This technique can be readily scalable and 112 MSCs could be produced within 30 min or less. By virtue of open inner porous network and high electrical conductivity of the porous graphene films, laser-scribed graphene MSCs delivered a volumetric capacitance of 3.05 F/cm³ at 16.8 mA/cm², maintained 60% of initial capacitance even operated at an ultrahigh current density of 1.84×10^4 mA/cm². This current density is at least 2 orders of magnitude higher than the conventional SCs, indicative of excellent rate capability and high power density. Moreover, these MSCs displayed an ultrahigh stacked power density of ~ 200 W/cm³ measured at ionic liquid electrolyte with a voltage of 2.5 V. These extraordinary results are well explained by (i) tremendous reduction of ion diffusion pathway between two microelectrodes and (ii) remarkably miniaturized resistance of ion diffusion from electrolyte to graphene surface due to open porous network structure.

Recently, our group [8] also exploited another approach of scalable fabrication of graphene-based MSCs under the assistance of UV light for efficient reduction and direct patterning of GO film (Fig. 12a and 12b). First, thin films of GO/TiO₂ nanoparticles were achieved by vacuum filtration of GO and TiO₂ dispersion, and then the obtained hybrid films covered by a customized photomask were synchronously reduced and patterned under the exposure at UV irradiation. It should be emphasized that this photo-reduction strategy does not require precise equipment, expensive materials and clean room operations, and the as-prepared planar MSCs could be tailored into different shapes with desirable device geometries and sizes (Fig. 12c–12i). Note that the TiO₂ nanoparticles in the composite films can act as both an active pseudocapacitive material and nanospace fillers, preventing the restacking of graphene sheets, consequently resulting in remarkably boosting the electrochemical performance of the MSCs. As expected, these MSCs could be stably operated in ionic liquid with a high scan rate of 200 V/s at a cell voltage of 3 V, due to the advantages of the planar hybrid films and superior wettability between the hybrid films and electrolyte (Fig. 12j and 12k). Most importantly, the MSCs showed a high volumetric energy density of 7.7 mWh/cm³, outstanding power density of 312 W/cm³, excellent flexibility and cycling stability (Fig. 12l).

Interfacial integration of the shape-engineered electrode with strongly bonded current collector is crucial for minimizing both

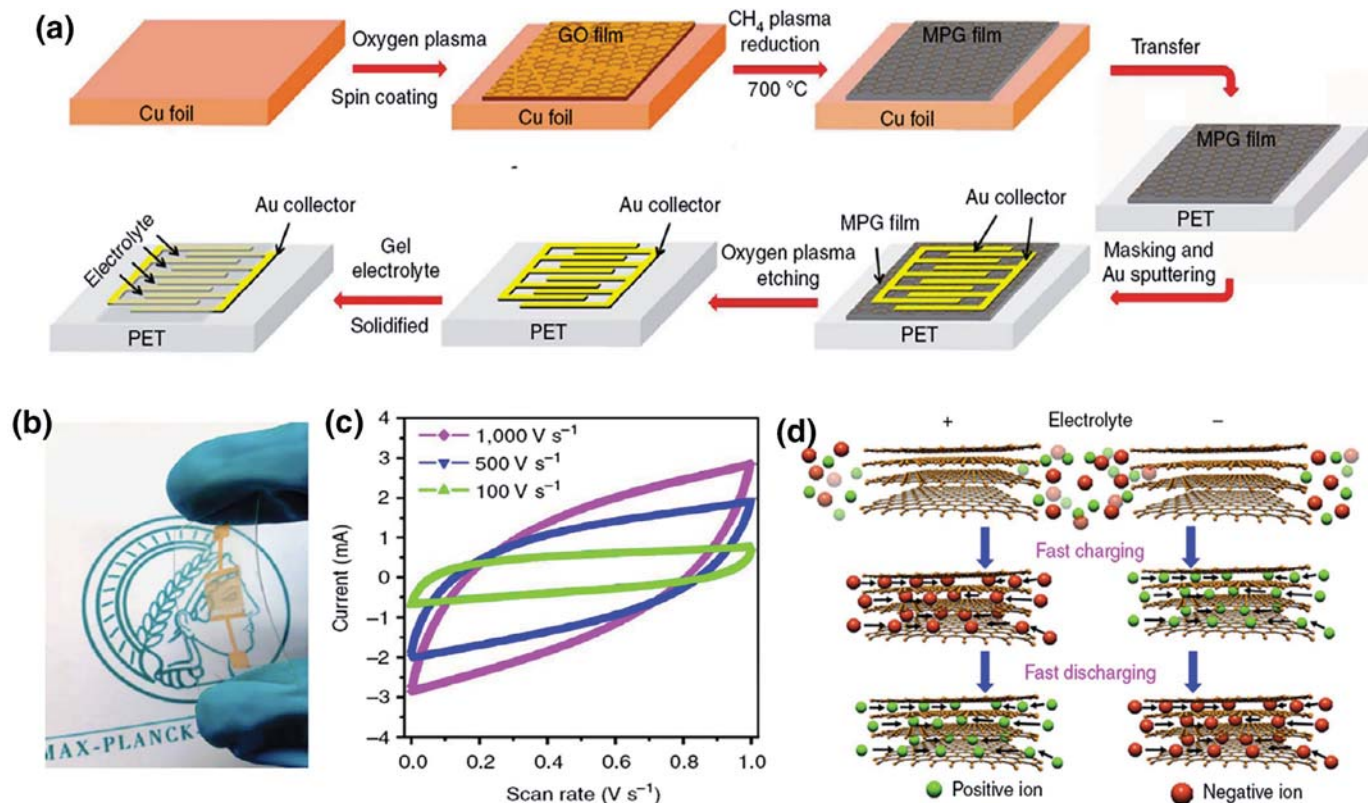


Fig. 11. (a) Schematic of fabrication of flexible MSCs. (b) A photograph of MSCs with bending state. (c) CV curves of MSCs obtained at scan rates from 100 to 1000 V/s. (d) Planar geometry of MSCs, showing the transportation of ions along the planar graphene nanosheets with a short diffusion length. Reprinted from Ref. [17] with permission of Nature publishing group.

ionic and electronic resistance, and then developing high-power SCs. Generally, the conventional SCs have the weak interfacial contact between current collectors and active electrode films in a typical physical fashion, significantly reducing the rate of electron transfer, and thus resulting in poor rate capability. Recently, our group [125] reported the rational construction of high-power MSCs using vertically aligned graphene (VG) nanosheets with strong interaction to current collector, derived from thermally decomposed conductive SiC substrate (Fig. 13a). The as-grown VG arrays displayed a standing basal plane on the SiC substrate, tailored thickness of 3.5 μm and 28 μm , high density ordering alignment of graphene with high quality, open inter-sheet channels and excellent electrical conductivity of 192 S/cm (Fig. 13b–13d). The obtained VG with strong bonding to the SiC substrates were directly assembled into MSCs without any further treatment and the requirement of metal current collectors. As a result, the assembled MSCs showed a high scan rate up to 200 V/s in both aqueous gel electrolyte and ionic liquid systems, exhibiting a superior areal capacitance of 7.3 mF/cm², fast frequency response with a short time constant of 9 ms and high power density of 61 W/cm³ (Fig. 13e–13g), which is much better than that of VG based MSCs with relatively weak contact of VG and substrate [126]. These outstanding results are mainly ascribed to the seamless integration of VG arrays strongly bonding with the current collector of SiC substrate and open inter-sheet channels with edge-enriched structure, which is key for minimizing the contact resistance, endowing both rapid ion and electron transport for ultrafast charge-discharge process.

3.4. Arbitrary-shape planar sandwich supercapacitors

To date, most reported SCs are conventionally constructed based on two substrates with a sandwich-like stacked geome-

try, leading to the absence of versatility and integration, which is a significant yet important direction but still under-developed [54,127,128]. On the other hand, planar SCs with the interdigital configuration hold great promises for the superior flexibility, wearability and miniaturization of electronic devices, since two electrodes, electrolyte, current collectors and free separator are integrated on the same in-plane substrate [4,112,113,129]. To avoid short circuit, the neighboring electrodes in such planar geometry are usually separated by an empty interspace. Therefore, one major drawback of this planar structure is that the positive and negative electrodes cannot absolutely intersect each other to construct arbitrary-shaped planar SCs [17]. To overcome this obstacle, our group [130] creatively constructed graphene-based planar sandwich SCs with superior flexibility and arbitrary-shaped property, bridging the gap between sandwich and planar SCs.

As shown in Fig. 14(a), the arbitrary-shaped planar sandwich SCs represented in junction-wire shape were fabricated through continuously printing EG ink as electrodes and nanosized graphene oxide (NGO) ink as a separator to design the shape-designable EG/NGO/EG sandwich-like structured film with the help of alternating customized masks (Fig. 14b and 14c). Moreover, various shapes of rectangle, “A” letter, “1” and “2” numbers, hollow-square and circle were also designed using the same strategy with assistance of the distinct customized masks. Note that the thickness of NGO is only 2 μm , much thinner than the commercial separator of $\sim 11 \mu\text{m}$. In addition, such planar sandwich SCs can be readily self-interconnected in series and/or parallel without the requirement of metal connects through elaborated layout of the homemade masks (Fig. 14d). The as-fabricated junction-wire-shaped SCs showed excellent mechanical flexibility, with 93% of its initial capacitance retained after repeated bending for 1000 times, and exceptional cycling stability without obvious capacitance degradation

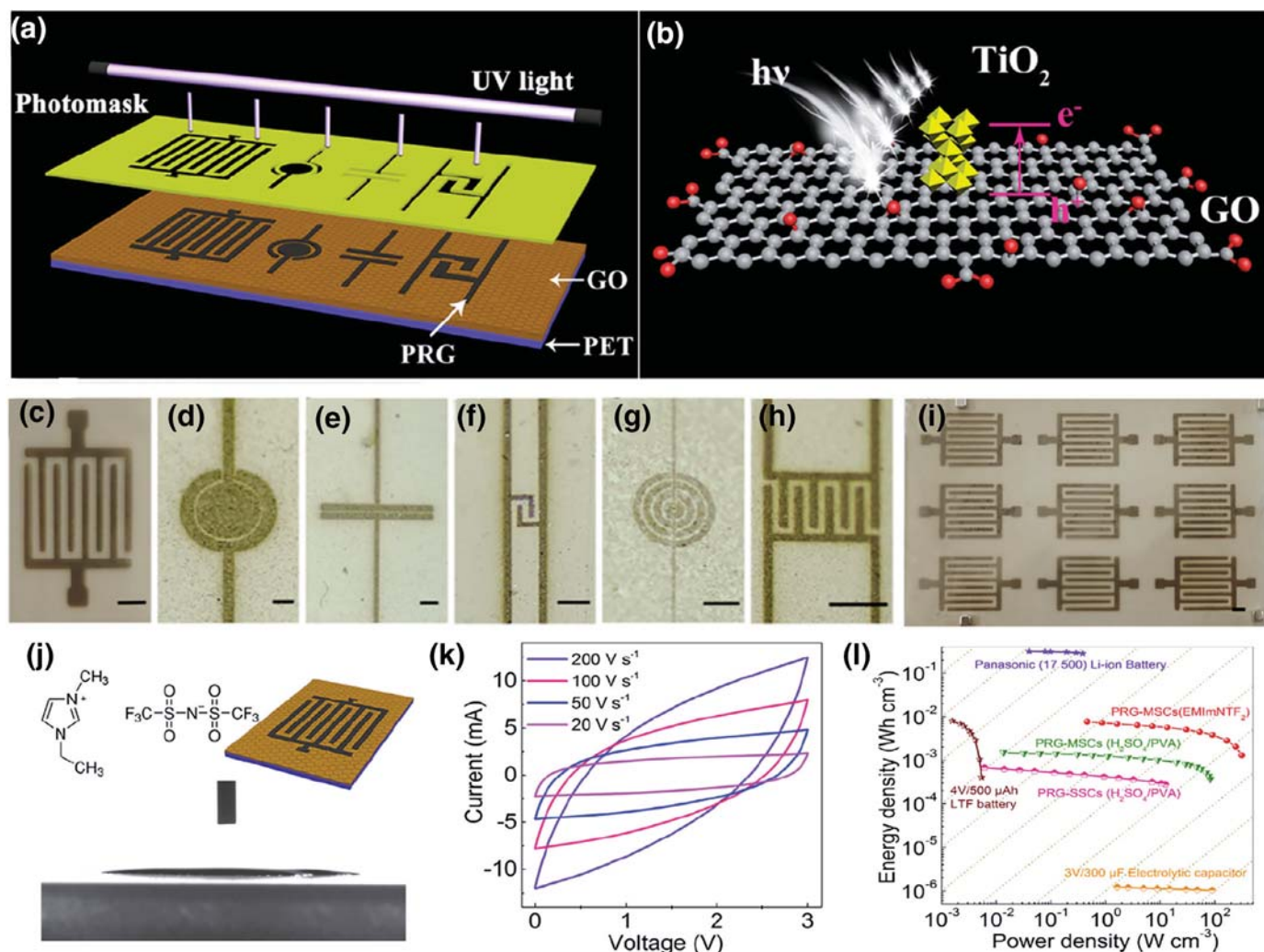


Fig. 12. (a) Schematic of the fabrication process of MSCs from photoreduced GO/TiO₂ hybrid films with the assistance of the photomask at the exposure of UV light. (b) Photochemical reduction mechanism of GO film under the interaction of ultraviolet irradiation with the catalysis of TiO₂ nanoparticle. (c–i) Various MSCs with different sizes and shapes of (c) parallel interdigital, (d) concentric circular, (e) parallel strip, (f) folding line, (g) circular interdigital (h) small-sized planar interdigital, (i) 9 parallel interdigital MSCs on one single polyethylene terephthalate (PET) substrate. Scale bar of (c, i) is 250 μm , scale bar of (d–h) is 500 μm . (j) Scheme of MSCs (top right), molecular structure of 1-ethyl-3-methylimidazolium bis (trifluoromethylsulfonyl) imide (EMIMNTF₂) (top left), and contact angle of EMIMNTF₂ on the surface of the photo-reduction graphene film (bottom). (k) CV curves of MSCs at ionic liquid of EMIMNTF₂. (l) Ragone plot of MSCs. Reprinted from Ref. [8] with permission of American Chemical Society.

after 1000 cycles under continuous bending state (Fig. 14e–14g). Remarkably, eight circle-shaped SCs self-interconnected in series can be well worked at a high cell voltage of 6.4 V, indicating the output voltage and current can be modulated for designable integrated circuits of modular power source. Using this similar approach, our group [131] further constructed this new-type planar sandwich ASCs based on layer-stacked all-in-one monolithic film, in which 2D boron nitride (BN) nanosheets act as separator, EG nanosheets as negative electrode, and MnO₂ nanosheets as positive electrode, respectively, printed on one single flexible substrate (Fig. 14h). The voltage window of such planar sandwich ASCs can reach up to 1.8 V, much higher than that of symmetric SCs with only 0.8 V (Fig. 14i and 14j), suggestive of high energy density. Correspondingly, Ragone plot exhibited this ASCs possessed a much higher volumetric energy density of 8.6 mWh/cm³ in comparison with planar symmetric SCs based on EG or MnO₂. More importantly, these planar sandwich SCs with various shapes can be seamlessly integrated with electronic circuits.

Electrochemical performance of these planar sandwich SCs in both symmetric and asymmetric types will be intensively enlarged,

through further exploitation of advanced materials as both high-capacitance active electrodes, superior ionic conductive separators, and high-voltage all-solid-state electrolyte. Furthermore, this strategy for fabricating planar sandwich SCs is highly flexible and compatible with various high-resolution printing techniques, e.g., inkjet printing, 3D printing, for mass production of printable planar energy storage devices.

4. Perspectives and challenges

The recent progress of different emerging graphene-based materials, such as graphene, porous graphene, 2D graphene-based hybrid nanosheets, 3D graphene-based framework, graphene fibers and graphene films, was summarized as high-performance electrode candidates in EDLCs, pseudocapacitors, HSCs, FSCs, MSCs, high-voltage SCs, and new-type planar sandwich SCs. The key intrinsic properties of high SSA, high theoretical capacitance (550 F/g), excellent electrical conductivity and superior mechanical flexibility of graphene enable it to be a huge potential as flexible, wearable, miniaturized and planar electrodes for next-generation

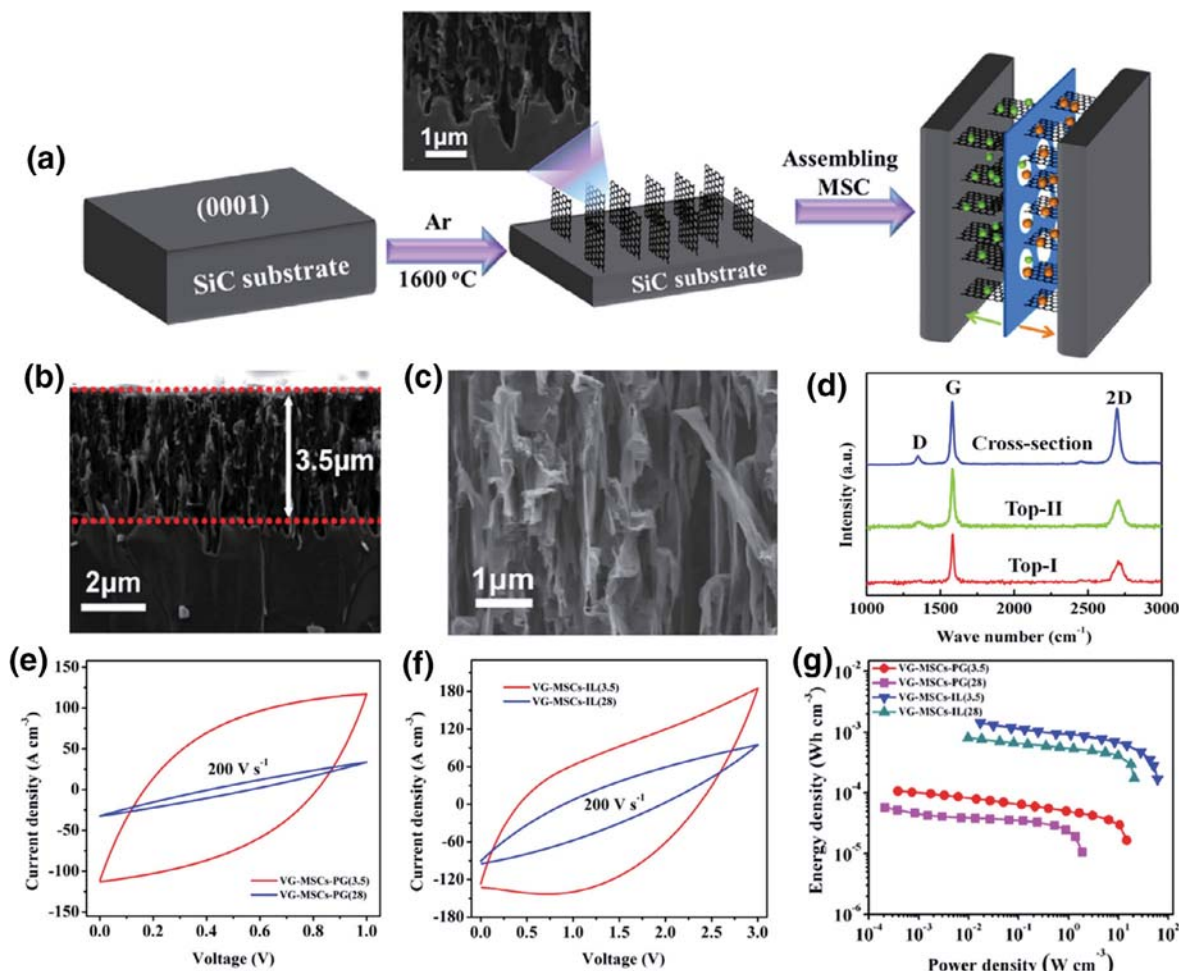


Fig. 13. (a) Schematic illustration of as-grown VG arrays via directly thermal decomposition of SiC and assembled MSCs. (b) Cross-section SEM image of VG with a thickness of 3.5 μm . (c) Cross-section SEM image with high magnification. (d) Raman spectra. (e) CV curves in aqueous gel electrolyte at a scan rate of 200 V/s. (f) CV curves in ionic liquid measured at a scan rate of 200 V/s. (g) Ragone plot of VG-MSCs. Reprinted from Ref. [125] with permission of American Chemical Society.

SCs, and to satisfy the demands of flexible, multifunctional and smart electronic devices. Nevertheless, enormous development of novel graphene nanostructures with high packing density, outstanding electrical conductivity among graphene sheets for reducing the contact resistance, optimized hierarchical porosity allowing for effective and rapid ion transport, and large accessible surface area as well as innovation of device geometry, electrolyte and interfacial engineering are specially needed to further enlarge both power density and energy density of these graphene-based next-generation SCs.

Several crucial challenging issues are still urgently unsolved as follows. (i) The first key challenge lies in the controllable preparation of high-quality graphene products in terms of designable number of layers, surface properties, lateral sizes, defects and conductivity, which is the prerequisite condition for further energy storage applications. (ii) Considering the practical applications, the second issue needed to be addressed well is how to carry out large-scale fabrication of graphene-based materials with desired composition and nano-architectures and high SAA at low cost for targeted SC applications. For instance, nanoporous and continuous graphene films is possibly to be the right one for flexible or planar SCs and MSCs, and similarly, graphene-based fibers for 1D flexible, wearable FSCs, while nanoporous and highly conductive graphene powder synthesized by chemical activation could be the best choice for high-energy bulk SCs. Alternatively, graphene can serve as the composite carrier with metal oxide or conduc-

tive polymers for high-performance HSCs. Therefore, different-type graphene products should be reasonably chosen taking into consideration of their corresponding SCs with varying functions. Moreover, continuous investigation on graphene-based various nanostructures should be further implemented to achieve highly active components and controlled open conductive networks. (iii) As a versatile building block, graphene with different nanostructure and sizes, and their derivatives of 1D fibers, 2D films, 3D porous networks could be designed into various hybrid materials with specific functionalities, so a key issue considered numerously is how to simultaneously achieve high volumetric and gravimetric capacitances of these SCs through rational design of graphene-based electrodes. In short, how to increase the packing density of graphene-based materials without influencing the electrochemical capacitive behaviors of device through rational approach is the key issue we are still facing. (iv) Systematical screening and interfacial integrity of the main device components, including graphene-based electrodes, electrolyte, current collectors, separator, substrate and package, is the core part for high-performance SCs through processing the optimized interfacial interactions of electrode and electrolyte, fabricating well-defined graphene-based nanostructures to enhance ion diffusion and electron transfer, and consequently achieving high cell voltage as well as high capacitance and rate capability in a single device. Specifically, improving the comprehensive performance of SCs is dependent not only on the intrinsic properties of graphene electrode materials, but also

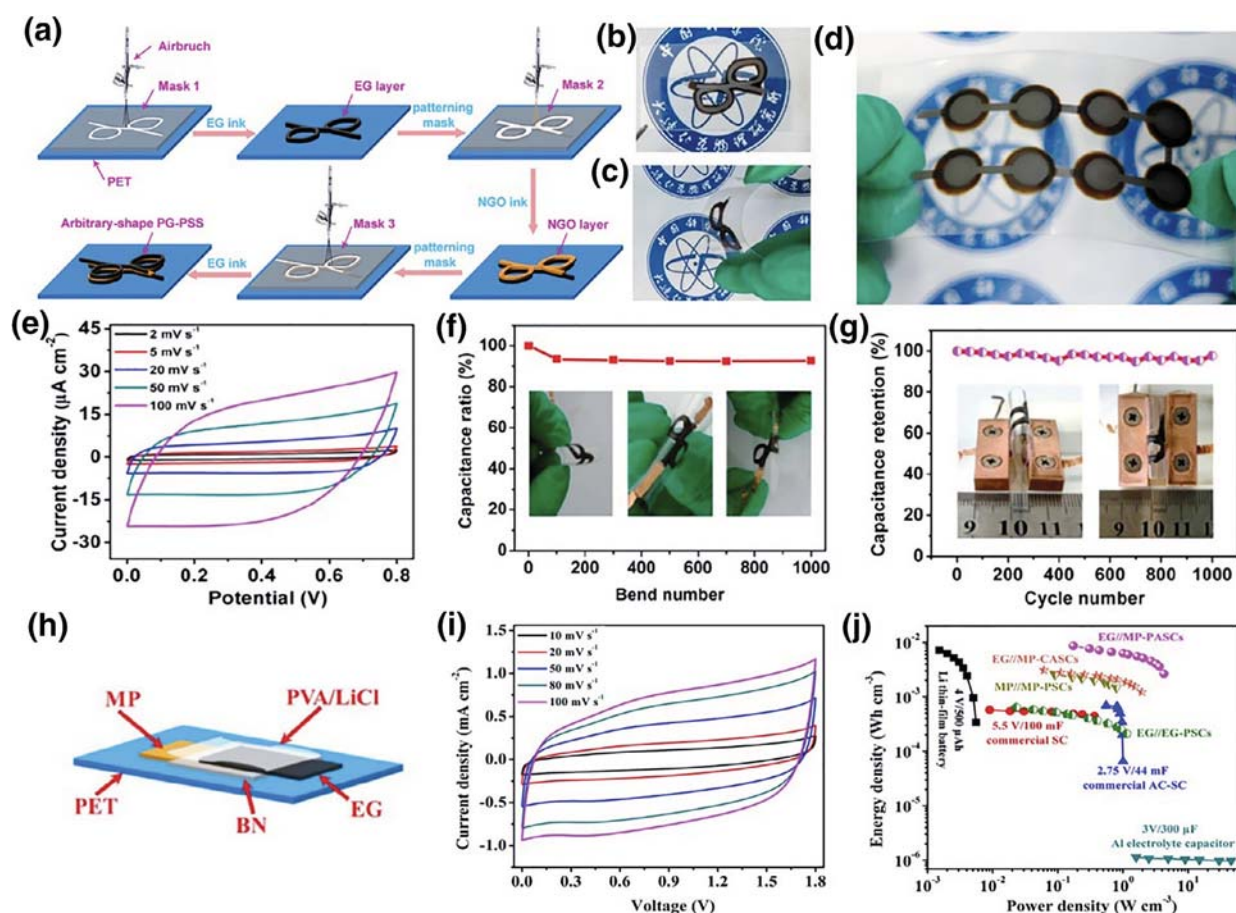


Fig. 14. (a) Schematic diagram of the fabrication of arbitrary-shaped SCs (junction-wire-shaped) constructed with an EG/NGO/EG layer structured film on one flexible PET substrate. (b, c) Optical images of the junction-wire-shaped SCs with flat (b) and bent (c) states. (d) Optical image of eight circle-shaped SCs self-interconnected in series under the bending state. (e) CV curves of the junction-wire-shaped SCs. (f) Capacitance ratio as a function of the repeated bending number. (g) Capacitance retention under the continuous bending condition. Reprinted from Ref. [130] with permission of American Chemical Society. (h) Schematic of the planar ASCs based on all-in-one monolithic film, using BN nanosheets as a separator. (i) CV curves of the planar ASCs. (j) Ragone plot of the planar ASCs. Reprinted from Ref. [131] with permission of Elsevier.

on the reasonable design, optimization, and compatible combination of each individual device component in the whole cell.

Acknowledgments

This work was financially supported by the National Natural Science Foundation of China (Grant 51572259), National Key R&D Program of China (Grant 2016YBF0100100 and 2016YFA0200200), Natural Science Foundation of Liaoning Province (Grant 201602737), Thousand Youth Talents Plan of China, DICP (DICP ZZBS201708), and Exploratory Research Projects of Shaanxi Yanchang Petroleum (Group) CO., LTD & DICP.

References

- [1] P. Simon, Y. Gogotsi, *Nat. Mater.* 7 (2008) 845–854.
- [2] Y. Zhai, Y. Dou, D. Zhao, P.F. Fulvio, R.T. Mayes, S. Dai, *Adv. Mater.* 23 (2011) 4828–4850.
- [3] X. Peng, L. Peng, C. Wu, Y. Xie, *Chem. Soc. Rev.* 43 (2014) 3303–3323.
- [4] Z.S. Wu, X. Feng, H.M. Cheng, *Natl. Sci. Rev.* 1 (2014) 277–292.
- [5] Y. Yoon, K. Lee, H. Lee, *Nanotechnology* 27 (2016) 172001.
- [6] L. Liu, Z. Niu, J. Chen, *Chem. Soc. Rev.* 45 (2016) 4340–4363.
- [7] Y. Shao, M.F. El-Kady, L.J. Wang, Q. Zhang, Y. Li, H. Wang, M.F. Mousavi, R.B. Kaner, *Chem. Soc. Rev.* 44 (2015) 3639–3665.
- [8] S. Wang, Z.S. Wu, S. Zheng, F. Zhou, C. Sun, H.M. Cheng, X. Bao, *ACS Nano* 11 (2017) 4283–4291.
- [9] Y. Fu, X. Cai, H. Wu, Z. Lv, S. Hou, M. Peng, X. Yu, D. Zou, *Adv. Mater.* 24 (2012) 5713–5718.
- [10] Y. Meng, Y. Zhao, C. Hu, H. Cheng, Y. Hu, Z. Zhang, G. Shi, L. Qu, *Adv. Mater.* 25 (2013) 2326–2331.
- [11] H. Zhang, *ACS Nano* 9 (2015) 9451–9469.
- [12] K.S. Novoselov, A.K. Geim, S.V. Morozov, D. Jiang, Y. Zhang, S.V. Dubonos, I.V. Grigorieva, A.A. Firsov, *Science* 306 (2004) 666–669.
- [13] D. Wu, F. Zhang, H. Liang, X. Feng, *Chem. Soc. Rev.* 41 (2012) 6160–6177.
- [14] Y. Dong, Z.-S. Wu, W. Ren, H.-M. Cheng, X. Bao, *Sci. Bull.* 62 (2017) 724–740.
- [15] Y. Zhu, S. Murali, M.D. Stoller, K. Ganesh, W. Cai, P.J. Ferreira, A. Pirkle, R.M. Wallace, K.A. Cychoz, M. Thommes, *Science* 332 (2011) 1537–1541.
- [16] X. Yang, C. Cheng, Y. Wang, L. Qiu, D. Li, *Science* 341 (2013) 534–537.
- [17] Z.S. Wu, K. Parvez, X. Feng, K. Müllen, *Nat. Commun.* 4 (2013) 2487.
- [18] Z.S. Wu, Y.Z. Tan, S. Zheng, S. Wang, K. Parvez, J. Qin, X. Shi, C. Sun, X. Bao, X. Feng, K. Müllen, *J. Am. Chem. Soc.* 139 (2017) 4506–4512.
- [19] X. Zhang, X. Cheng, Q. Zhang, *J. Energy Chem.* 25 (2016) 967–984.
- [20] H.-J. Qiu, L. Liu, Y. Wang, *Sci. Bull.* 61 (2016) 443–450.
- [21] M.D. Stoller, S. Park, Y. Zhu, J. An, R.S. Ruoff, *Nano Lett.* 8 (2008) 3498–3502.
- [22] Z.S. Wu, Y. Sun, Y.Z. Tan, S. Yang, X. Feng, K. Müllen, *J. Am. Chem. Soc.* 134 (2012) 19532–19535.
- [23] L.L. Zhang, X. Zhao, M.D. Stoller, Y. Zhu, H. Ji, S. Murali, Y. Wu, S. Perales, B. Clevenger, R.S. Ruoff, *Nano Lett.* 12 (2012) 1806–1812.
- [24] L. Zhang, F. Zhang, X. Yang, G. Long, Y. Wu, T. Zhang, K. Leng, Y. Huang, Y. Ma, A. Yu, Y. Chen, *Sci. Rep.* 3 (2013) 1408.
- [25] Y. Gao, Y. Zhang, Y. Zhang, L. Xie, X. Li, F. Su, X. Wei, Z. Xu, C. Chen, R. Cai, *J. Energy Chem.* 25 (2016) 49–54.
- [26] Y. Zhang, J.-Y. Zhu, H.-B. Ren, Y.-T. Bi, L. Zhang, *Chin. Chem. Lett.* 28 (2017) 935–942.
- [27] G.-L. Tian, Q. Zhang, M.-Q. Zhao, H.-F. Wang, C.-M. Chen, F. Wei, *AIChE J.* 61 (2015) 747–755.
- [28] L. Wei, H.E. Karahan, S. Zhai, Y. Yuan, Q. Qian, K. Goh, A.K. Ng, Y. Chen, *J. Energy Chem.* 25 (2016) 191–198.
- [29] M. Li, Z. Wu, W. Ren, H. Cheng, N. Tang, W. Wu, W. Zhong, Y. Du, *Carbon* 50 (2012) 5286–5291.
- [30] Y.-Z. Liu, Y.-F. Li, F.-Y. Su, L.-J. Xie, Q.-Q. Kong, X.-M. Li, J.-G. Gao, C.-M. Chen, *Energy Storage Mater.* 2 (2016) 69–75.
- [31] Z.S. Wu, A. Winter, L. Chen, Y. Sun, A. Turchanin, X. Feng, K. Müllen, *Adv. Mater.* 24 (2012) 5130–5135.
- [32] X. Wang, M. Wang, X. Zhang, H. Li, X. Guo, *J. Energy Chem.* 25 (2016) 26–34.
- [33] X. Zhou, H. Li, J. Yang, *J. Energy Chem.* 25 (2016) 35–40.

- [34] C. Cui, W. Qian, Y. Yu, C. Kong, B. Yu, L. Xiang, F. Wei, J. Am. Chem. Soc. 136 (2014) 2256–2259.
- [35] Y. Gogotsi, P. Simon, Science 334 (2011) 917–918.
- [36] Y. Xu, Z. Lin, X. Zhong, X. Huang, N.O. Weiss, Y. Huang, X. Duan, Nat. Commun. 5 (2014) 4554.
- [37] Y. Yoon, K. Lee, S. Kwon, S. Seo, H. Yoo, S. Kim, Y. Shin, Y. Park, D. Kim, J.-Y. Choi, ACS Nano 8 (2014) 4580–4590.
- [38] Y. Xu, C.Y. Chen, Z. Zhao, Z. Lin, C. Lee, X. Xu, C. Wang, Y. Huang, M.I. Shakir, X. Duan, Nano Lett. 15 (2015) 4605–4610.
- [39] J.J. Yoo, K. Balakrishnan, J. Huang, V. Meunier, B.G. Sumpter, A. Srivastava, M. Conway, A.L. Reddy, J. Yu, R. Vajtai, P.M. Ajayan, Nano Lett. 11 (2011) 1423–1427.
- [40] S. Murali, N. Quarles, L.L. Zhang, J.R. Potts, Z. Tan, Y. Lu, Y. Zhu, R.S. Ruoff, Nano Energy 2 (2013) 764–768.
- [41] Y. Tao, X. Xie, W. Lv, D.M. Tang, D. Kong, Z. Huang, H. Nishihara, T. Ishii, B. Li, D. Golberg, F. Kang, T. Kyotani, Q.H. Yang, Sci. Rep. 3 (2013) 2975.
- [42] Z.-S. Wu, W. Ren, D.-W. Wang, F. Li, B. Liu, H.-M. Cheng, ACS Nano 4 (2010) 5835–5842.
- [43] Y. Liu, R. Wang, X. Yan, Sci. Rep. 5 (2015) 11095.
- [44] D.H. Nagaraju, Q. Wang, P. Beaujeu, H.N. Alshareef, J. Mater. Chem. A 2 (2014) 17146–17152.
- [45] J. Qin, Z.-S. Wu, F. Zhou, H. Dong, H. Xiao, S. Zheng, S. Wang, X. Shi, H. Huang, C. Sun, X. Bao, Chin. Chem. Lett. (2017) 1007, doi:10.1016/j.ccl.2017.1008.
- [46] F. Ran, Y. Yang, L. Zhao, X. Niu, D. Zhang, L. Kong, Y. Luo, L. Kang, J. Energy Chem. 24 (2015) 388–393.
- [47] Z.-S. Wu, D.-W. Wang, W. Ren, J. Zhao, G. Zhou, F. Li, H.-M. Cheng, Adv. Funct. Mater. 20 (2010) 3595–3602.
- [48] S. Liu, P. Gordiichuk, Z.S. Wu, Z. Liu, W. Wei, M. Wagner, N. Mohamed-Noriega, D. Wu, Y. Mai, A. Herrmann, K. Müllen, X. Feng, Nat. Commun. 6 (2015) 8817.
- [49] Z.S. Wu, K. Parvez, S. Li, S. Yang, Z. Liu, S. Liu, X. Feng, K. Müllen, Adv. Mater. 27 (2015) 4054–4061.
- [50] Z.S. Wu, Y. Zheng, S. Zheng, S. Wang, C. Sun, K. Parvez, T. Ikeda, X. Bao, K. Müllen, X. Feng, Adv. Mater. 29 (2017) 1602960.
- [51] Z.-S. Wu, Z. Liu, K. Parvez, X. Feng, K. Müllen, Adv. Mater. 27 (2015) 3669–3675.
- [52] B.-n. Zheng, C. Gao, New Carbon Mater. 31 (2016) 315–320.
- [53] M. Wang, Y.-X. Xu, Chin. Chem. Lett. 27 (2016) 1437–1444.
- [54] S. Zheng, Z.-S. Wu, S. Wang, H. Xiao, F. Zhou, C. Sun, X. Bao, H.-M. Cheng, Energy Storage Mater. 6 (2017) 70–97.
- [55] W. Zuo, C. Xie, P. Xu, Y. Li, J. Liu, Adv. Mater. (2017), doi:10.1002/adma.201703463.
- [56] J. Chen, J. Xu, S. Zhou, N. Zhao, C.-P. Wong, Nano Energy 15 (2015) 719–728.
- [57] Z. Fan, J. Yan, T. Wei, L. Zhi, G. Ning, T. Li, F. Wei, Adv. Funct. Mater. 21 (2011) 2366–2375.
- [58] Z. Zhang, F. Xiao, L. Qian, J. Xiao, S. Wang, Y. Liu, Adv. Energy Mater. 4 (2014) 1400064.
- [59] M.-C. Liu, Y.-M. Hu, W.-Y. An, L.-B. Kong, L. Kang, J. Energy Chem. 26 (2017) 750–756.
- [60] M. Liu, J. Li, W. Han, L. Kang, J. Energy Chem. 25 (2016) 601–608.
- [61] Y. Wang, W. Lai, N. Wang, Z. Jiang, X. Wang, P. Zou, Z. Lin, H.J. Fan, F. Kang, C.-P. Wong, C. Yang, Energy Environ. Sci. 10 (2017) 941–949.
- [62] Y. Jin, H. Chen, M. Chen, N. Liu, Q. Li, ACS Appl. Mater. Inter. 5 (2013) 3408–3416.
- [63] J. Yan, Z. Fan, W. Sun, G. Ning, T. Wei, Q. Zhang, R. Zhang, L. Zhi, F. Wei, Adv. Funct. Mater. 22 (2012) 2632–2641.
- [64] D.-L. Fang, Z.-D. Chen, X. Liu, Z.-F. Wu, C.-H. Zheng, Electrochim. Acta. 81 (2012) 321–329.
- [65] W. Sun, X. Rui, M. Ulaganathan, S. Madhavi, Q. Yan, J. Power Sources 295 (2015) 323–328.
- [66] L. Li, S. Peng, H.B. Wu, L. Yu, S. Madhavi, X.W.D. Lou, Adv. Energy Mater. 5 (2015) 1500753.
- [67] Z. Chen, V. Augustyn, J. Wen, Y. Zhang, M. Shen, B. Dunn, Y. Lu, Adv. Mater. 23 (2011) 791–795.
- [68] L. Ye, Q. Liang, Y. Lei, X. Yu, C. Han, W. Shen, Z.-H. Huang, F. Kang, Q.-H. Yang, J. Power Sources 282 (2015) 174–178.
- [69] H. Kim, K.Y. Park, J. Hong, K. Kang, Sci. Rep. 4 (2014) 5278.
- [70] E. Lim, C. Jo, M.S. Kim, M.-H. Kim, J. Chun, H. Kim, J. Park, K.C. Roh, K. Kang, S. Yoon, J. Lee, Adv. Funct. Mater. 26 (2016) 3711–3719.
- [71] J. Lv, T. Liang, M. Yang, S. Ken, M. Hideo, J. Energy Chem. 26 (2017) 330–335.
- [72] K. Leng, F. Zhang, L. Zhang, T. Zhang, Y. Wu, Y. Lu, Y. Huang, Y. Chen, Nano Res. 6 (2013) 581–592.
- [73] P. Han, W. Ma, S. Pang, Q. Kong, J. Yao, C. Bi, G. Cui, J. Mater. Chem. A 1 (2013) 5949–5954.
- [74] N. Yabuuchi, K. Kubota, M. Dahbi, S. Komaba, Chem. Rev. 114 (2014) 11636–11682.
- [75] Z. Chen, V. Augustyn, X. Jia, Q. Xiao, B. Dunn, Y. Lu, ACS Nano 6 (2012) 4319–4327.
- [76] S. Kajiyama, H. Iinuma, E. Hosono, S. Oro, I. Moriguchi, M. Okubo, A. Yamada, Nat. Commun. 6 (2015) 6544.
- [77] F. Wang, X. Wang, Z. Chang, X. Wu, X. Liu, L. Fu, Y. Zhu, Y. Wu, W. Huang, Adv. Mater. 27 (2015) 6962–6968.
- [78] Y. Ai, Z. Lou, S. Chen, D. Chen, Z.M. Wang, K. Jiang, G. Shen, Nano Energy 35 (2017) 121–127.
- [79] L. Liu, B. Shen, D. Jiang, R. Guo, L. Kong, X. Yan, Adv. Energy Mater. 6 (2016) 1600763.
- [80] Z. Lou, S. Chen, L. Wang, K. Jiang, G. Shen, Nano Energy 23 (2016) 7–14.
- [81] S. Pan, J. Ren, X. Fang, H. Peng, Adv. Energy Mater. 6 (2016) 1501867.
- [82] C. Chen, J. Cao, Q. Lu, X. Wang, L. Song, Z. Niu, J. Chen, Adv. Funct. Mater. 27 (2017) 1604639.
- [83] H. Sun, X. Fu, S. Xie, Y. Jiang, H. Peng, Adv. Mater. 28 (2016) 2070–2076.
- [84] J.Y. Tao, N.S. Liu, J.Y. Rao, L.W. Ding, M.RAL Bahrani, L.Y. Li, J. Su, Y.H. Gao, Nanoscale 6 (2014) 15073–15079.
- [85] F. Zhang, Y.H. Lu, X. Yang, L. Zhang, T.F. Zhang, K. Leng, Y.P. Wu, Y. Huang, Y.F. Ma, Y.S. Chen, Small 10 (2014) 2285–2292.
- [86] W. Chen, C. Xia, H.N. Alshareef, Nano Energy 15 (2015) 1–8.
- [87] H. Xiao, Z.S. Wu, L. Chen, F. Zhou, S. Zheng, W. Ren, H.M. Cheng, X. Bao, ACS Nano 11 (2017) 7284–7292.
- [88] D. Yu, Q. Qian, L. Wei, W. Jiang, K. Goh, J. Wei, J. Zhang, Y. Chen, Chem. Soc. Rev. 44 (2015) 647–662.
- [89] L. Chen, Y. Liu, Y. Zhao, N. Chen, L. Qu, Nanotechnology 27 (2016) 032001.
- [90] F. Meng, Q. Li, L. Zheng, Energy Storage Mater. 8 (2017) 85–109.
- [91] Z. Xu, C. Gao, Nat. Commun. 2 (2011) 571.
- [92] Z. Xu, H. Sun, X. Zhao, C. Gao, Adv. Mater. 25 (2013) 188–193.
- [93] H. Cheng, C. Hu, Y. Zhao, L. Qu, NPG Asia Mater. 6 (2014) 113 e.
- [94] Z. Li, Z. Xu, Y. Liu, R. Wang, C. Gao, Nat. Commun. 7 (2016) 13684.
- [95] G. Xin, T. Yao, H. Sun, S.M. Scott, D. Shao, G. Wang, J. Lian, Science 349 (2015) 1083–1087.
- [96] D. Yu, K. Goh, H. Wang, L. Wei, W. Jiang, Q. Zhang, L. Dai, Y. Chen, Nat. Nanotechnol. 9 (2014) 555–562.
- [97] J. Li, J. Li, L. Li, M. Yu, H. Ma, B. Zhang, J. Mater. Chem. A 2 (2014) 6359–6362.
- [98] E.Y. Jang, J. Carretero-Gonzalez, A. Choi, W.J. Kim, M.E. Kozlov, T. Kim, T.J. Kang, S.J. Baek, D.W. Kim, Y.W. Park, R.H. Baughman, Y.H. Kim, Nanotechnology 23 (2012) 235601.
- [99] R. Cruz-Silva, A. Morelos-Gomez, H.-i. Kim, H.-k. Jang, F. Tristan, S. Vega-Diaz, L.P. Rajukumar, A.L. Elías, N. Perea-Lopez, J. Suhr, ACS Nano 8 (2014) 5959–5967.
- [100] C. Hu, X. Zhai, L. Liu, Y. Zhao, L. Jiang, L. Qu, Sci. Rep. 3 (2013) 2065.
- [101] Z. Xu, C. Gao, Mater. Today 18 (2015) 480–492.
- [102] H.P. Cong, X.C. Ren, P. Wang, S.H. Yu, Sci. Rep. 2 (2012) 613.
- [103] H. Guo, M.-H. Yeh, Y.-C. Lai, Y. Zi, C. Wu, Z. Wen, C. Hu, Z.L. Wang, ACS Nano 10 (2016) 10580–10588.
- [104] Z. Dong, C. Jiang, H. Cheng, Y. Zhao, G. Shi, L. Jiang, L. Qu, Adv. Mater. 24 (2012) 1856–1861.
- [105] L. Kou, T. Huang, B. Zheng, Y. Han, X. Zhao, K. Gopalsamy, H. Sun, C. Gao, Nat. Commun. 5 (2014) 3754.
- [106] B. Wang, X. Fang, H. Sun, S. He, J. Ren, Y. Zhang, H. Peng, Adv. Mater. 27 (2015) 7854–7860.
- [107] M. Khalid, A.M.B. Honorato, J. Energy Chem. (2017) doi:10.1016/j.jchem.2017.1006.1011.
- [108] Y. Huang, H. Hu, Y. Huang, M. Zhu, W. Meng, C. Liu, Z. Pei, C. Hao, Z. Wang, C. Zhi, ACS Nano 9 (2015) 4766–4775.
- [109] W.K. Chee, H.N. Lim, Y. Andou, Z. Zainal, A.A.B. Hamra, I. Harrison, M. Al-tarawneh, Z.T. Jiang, N.M. Huang, J. Energy Chem. 26 (2017) 790–798.
- [110] X. Li, T. Zhao, Q. Chen, P. Li, K. Wang, M. Zhong, J. Wei, D. Wu, B. Wei, H. Zhu, Phys. Chem. Chem. Phys. 15 (2013) 17752–17757.
- [111] H. Wang, Q. Hao, X. Yang, L. Lu, X. Wang, Electrochem. Commun. 11 (2009) 1158–1161.
- [112] N.A. Kyeremateng, T. Brousse, D. Pech, Nat. Nanotechnol. 12 (2017) 7–15.
- [113] D. Qi, Y. Liu, Z. Liu, L. Zhang, X. Chen, Adv. Mater. 29 (2017) 1602802.
- [114] Z.-S. Wu, K. Parvez, X. Feng, K. Müllen, J. Mater. Chem. A 2 (2014) 8288–8293.
- [115] G.P. Xiong, C.Z. Meng, R.G. Reifenger, P.P. Irazoqui, T.S. Fisher, Electroanalysis 26 (2014) 30–51.
- [116] M.F. El-Kady, Y. Shao, R.B. Kaner, Nat. Rev. Mater. 1 (2016) 16033.
- [117] S. Wang, S.H. Zheng, C.L. Sun, Z.S. Wu, Sci. Sin. Chim. 46 (2016) 732–744.
- [118] Z. Liu, Z.S. Wu, S. Yang, R. Dong, X. Feng, K. Müllen, Adv. Mater. 28 (2016) 2217–2222.
- [119] T. Palaniselvam, J.-B. Baek, 2D Mater. 2 (2015) 032002.
- [120] X. Pu, M. Liu, L. Li, S. Han, X. Li, C. Jiang, C. Du, J. Luo, W. Hu, Z.L. Wang, Adv. Energy Mater. 6 (2016) 1601254.
- [121] W. Yang, M. Ni, X. Ren, Y. Tian, N. Li, Y. Su, X. Zhang, Curr. Opin. Colloid Interface 20 (2015) 416–428.
- [122] J. Chang, S. Adhikari, T.H. Lee, B. Li, F. Yao, D.T. Pham, V.T. Le, Y.H. Lee, Adv. Energy Mater. 5 (2015) 1500003.
- [123] M.F. El-Kady, V. Strong, S. Dubin, R.B. Kaner, Science 335 (2012) 1326–1330.
- [124] M.F. El-Kady, R.B. Kaner, Nat. Commun. 4 (2013) 1475.
- [125] S. Zheng, Z. Li, Z.S. Wu, Y. Dong, F. Zhou, S. Wang, Q. Fu, C. Sun, L. Guo, X. Bao, ACS Nano 11 (2017) 4009–4016.
- [126] D. Aradilla, M. Delaunay, S. Sadki, J.-M. Gerard, G. Bidan, J. Mater. Chem. A 3 (2015) 19254–19262.
- [127] H. Wu, Y. Zhang, L. Cheng, L. Zheng, Y. Li, W. Yuan, X. Yuan, Energy Storage Mater. 5 (2016) 8–32.
- [128] H.R. Paul, L. Dai, Natl. Sci. Rev. 4 (2017) 453–489.
- [129] L. Liu, Z. Niu, J. Chen, Nano Res. 10 (2017) 1524–1544.
- [130] S. Zheng, X. Tang, Z.S. Wu, Y.Z. Tan, S. Wang, C. Sun, H.M. Cheng, X. Bao, ACS Nano 11 (2017) 2171–2179.
- [131] S. Zheng, W. Lei, J. Qin, Z.-S. Wu, F. Zhou, S. Wang, X. Shi, C. Sun, Y. Chen, X. Bao, Energy Storage Mater. 10 (2018) 24–31.